REPORT DOCUMENTATION PAGE

Form Approved
OMB No. 0704-0188

1. AGENCY USE ONLY (Leave blank)	2. REPORT DATE	3. REPORT TYPE AND DATES COVERED
	24 June, 1996	Technical 6/1/95 - 5/31/96

4. TITLE AND SUBTITLE
Polymeric Self-Assembled Monolayers. 4. Synthesis, Characterization, and Stablity of ω-Functionalized, Self-Assembled Diacetylenic and Polydiacetyic Monolayers.

5. FUNDING NUMBERS
N00014-93-1-1338
300x084yip
96PR0-1027

6. AUTHOR(S)
T. Kim, K. C. Chan, R. M. Crooks, Q. Ye, L. Sun

7. PERFORMING ORGANIZATION NAME(S) AND ADDRESS(ES)
Department of Chemistry
Texas A&M University
College Station, Texas 77843-3255

8. PERFORMING ORGANIZATION REPORT NUMBER
21

9. SPONSORING/MONITORING AGENCY NAME(S) AND ADDRESS(ES)
Office of Naval Research
800 North Quincy Street
Arlington, Virginia 22217-5000

11. SUPPLEMENTARY NOTES
J. Am. Chem. Soc., submitted.

12a. DISTRIBUTION/AVAILABILITY STATEMENT
Reproduction in whole, or in part, is permitted for any purpose of the United States Government. This document has been approved for public release and sale; it's distribution is unlimited.

12b. DISTRIBUTION CODE

13. ABSTRACT *(Maximum 200 words)*

Here we discuss the preparation and characterization of photopolymerizable, self-assembled monolayers (SAMs) that consist of acid-, hydroxyl-, and methyl-terminated *n*-alkylthiols containing a diacetylene group ($HS(CH_2)_{10}C{\equiv}CC{\equiv}C(CH_2)_{10}X$; X=COOH, CH_2OH, and CH_3, respectively). The acid and hydroxyl surfaces are readily amenable to further synthetic elaboration, while the methyl-terminated SAM results in a clean, low-energy surface. As demonstrated by Fourier transform infrared external reflectance spectroscopy (FTIR-ERS), surface-enhanced Raman spectroscopy (SERS), ellipsometry, UV-vis spectroscopy, and electrochemical methods, all three materials self assemble onto Au surface to form ordered monolayers that can be photopolymerized with UV light. The polymerized SAMs are extremely durable compared to simple *n*-alkanethiol SAMs. For example, they are stable to electrochemical cycling, thermal excursions to 200 °C, and exposure to hot base (1:1 mixture of ethanol and 1.0 M aqueous KOH at 100 °C). All of these conditions completely strip *n*-alkanethiol SAMs from Au substrates. These high-performance materials are suitable for applications in lubrication, adhesion, corrosion inhibition, and chemical sensing.

14. SUBJECT TERMS			15. NUMBER OF PAGES 60
			16. PRICE CODE
17. SECURITY CLASSIFICATION OF REPORT	18. SECURITY CLASSIFICATION OF THIS PAGE	19. SECURITY CLASSIFICATION OF ABSTRACT	20. LIMITATION OF ABSTRACT
Unclassified	Unclassified	Unclassified	

[Prepared for Publication as an Article in *J. Am. Chem. Soc.*]

Polymeric Self-Assembled Monolayers. 4. Synthesis, Characterization, and Stability of ω-Functionalized, Self-Assembled Diacetylenic and Polydiacetylenic Monolayers

Taisun Kim*,[2]

Department Of Chemistry

Hallym University

Chuncheon, Kang-Won Do, 200-702, South Korea

[2]e-mail: tskim@sun.hallym.ac.kr

Kwok C. Chan and Richard M. Crooks*,[1]

Department of Chemistry

Texas A&M University

College Station, Texas 77843-3255

[1]e-mail: crooks@chemvx.tamu.edu

Qi Ye and Li Sun*,[3]

Department of Chemistry

University of Minnesota

Minneapolis, MN 55455-0431

[3]e-mail: sun@chemsun.chem.umn.edu

* Authors to whom correspondence should be addressed.

Submitted: 23 May, 1996

Abstract

Here we discuss the preparation and characterization of photopolymerizable, self-assembled monolayers (SAMs) that consist of acid-, hydroxyl-, and methyl-terminated *n*-alkylthiols containing a diacetylene group ($HS(CH_2)_{10}C{\equiv}CC{\equiv}C(CH_2)_{10}X$; X=COOH, CH_2OH, and CH_3, respectively). The acid and hydroxyl surfaces are readily amenable to further synthetic elaboration, while the methyl-terminated SAM results in a clean, low-energy surface. As demonstrated by Fourier transform infrared external reflectance spectroscopy (FTIR-ERS), surface-enhanced Raman spectroscopy (SERS), ellipsometry, UV-vis spectroscopy, and electrochemical methods, all three materials self assemble onto Au surface to form ordered monolayers that can be photopolymerized with UV light. The polymerized SAMs are extremely durable compared to simple *n*-alkanethiol SAMs. For example, they are stable to electrochemical cycling, thermal excursions to 200 °C, and exposure to hot base (1:1 mixture of ethanol and 1.0 M aqueous KOH at 100 °C). All of these conditions completely strip *n*-alkanethiol SAMs from Au substrates. These high-performance materials are suitable for applications in lubrication, adhesion, corrosion inhibition, and chemical sensing.

Introduction

In this paper we discuss the preparation and characterization of photopolymerizable, self-assembled monolayers (SAMs) that consist of methyl-, hydroxyl-, and acid-terminated *n*-alkylthiols containing a diacetylene group. In previous papers in this series, we described the synthesis of the monomers,[1] and showed that SAMs prepared from them can be used as ultrathin photoresists.[2] We have also shown that diacetylenic SAMs can be pillared by sequential polymerization and grafting steps to yield ordered, multilayer structures.[3] In forthcoming papers we will discuss the viscoelastic and mechanical properties of the mono- and multilayers measured using thickness-shear mode resonators[4] and interfacial force microscopy (IFM).[5-7] However, we confine ourselves here to a comparison of the IR, Raman, and UV-vis spectroscopic and electrochemical properties of these materials, and we compare the stability of the polymerized and unpolymerized diacetylenic SAMs to simple *n*-alkanethiol SAMs.

Monolayer and multilayer self-assembly chemistry is useful for preparing well-ordered organic surfaces.[8-11] A particularly popular and versatile version of monolayer self-assembly occurs when a Au substrate contacts a dilute vapor[12] or solution of a suitable organomercaptan.[9,11,13] This treatment results in a surface-adsorbed monolayer possessing well-defined chemical and physical properties, which have been characterized by contact-angle measurements, electrochemical methods, FTIR-external reflection spectroscopy (FTIR-ERS), ellipsometry, scanning probe microscopy, ultrahigh vacuum (UHV) surface spectroscopy, and other

techniques.[9,11] An excellent summary of these studies recently appeared,[9] but we briefly recount here some of the important physical and chemical aspects of organomercaptan SAMs that are relevant to our study.

It is generally accepted that organomercaptan SAMs assume a $(\sqrt{3} \times \sqrt{3})R30°$ overlayer structure on Au(111) and that adsorption occurs at surface three-fold hollow sites.[9,14] Since many Au surfaces have a pronounced (111) texture, the $(\sqrt{3} \times \sqrt{3})R30°$ structure is often assumed to be common to all Au substrates, including vapor-deposited films and polycrystalline wires and foils. Organomercaptans are thought to interact with Au according to eq 1. The resulting $Au(\delta^+)/HS(\delta^-)$ interaction has an energy of

$$Au + SH\text{-}R \;\text{-->}\; Au(\delta^+)/HS^{(\delta^-)}\text{-}R \qquad (1)$$

about 44 kcal/mol and the SAM is further stabilized by intermolecular van der Waals interactions.[9] Spectroscopic studies indicate that methyl-terminated *n*-alkanethiol SAMs are composed of hydrocarbon chains tilted 30-40° from the surface normal and twisted ~50° about the carbon backbone. SAMs formed from shorter chains are typically, but not always,[15] more disordered than those formed from longer-chain molecules. Defects within ordered domains are thought to result primarily from gauche conformations within the lower energy all-trans, extended SAM structure. More significant defects arise at grain, rotational, and antiphase boundaries as well as at stacking faults.[15]

SAMs are fairly robust under normal laboratory conditions and an additional hydrophobic interaction further increases the stability of SAMs terminated with hydrophobic groups in aqueous solutions. However, at extreme pHs,[16] in many nonaqueous solvents,[17] in the presence of molecules that compete for surface sites (such as Cl^-, CN^-, or other thiols),[2,18] at elevated temperatures,[19] or at extreme electrode potentials,[20,21] SAMs reveal their less-than-covalent binding interaction with the surface. While this instability has not significantly affected fundamental chemical and structural studies of SAMs, it has greatly limited their potential technological applications. Thus, while organomercaptan SAMs are useful for lithographic purposes[19,22-28] and as chemically sensitive interfaces for chemical sensors,[29] some other obvious applications such as corrosion inhibition,[30] lubrication,[31] and adhesion[7] have not generally been forthcoming. To improve substrate adherence and enhance the durability of SAMs, we have prepared diacetylenic SAMs that can be polymerized in the plane parallel to the substrate with UV light. Besides improving durability, we have been surprised to learn that polymerized SAMs are better barriers to transfilm mass transfer than the unpolymerized monolayers, which suggests that polymerization occurs topochemically; that is, with minimal change in orientation and free volume.

Polymerization of diacetylenes in the solid state was first reported by Wegner[32] and has subsequently been discussed in detail by others.[33-35] In contrast to the extended conjugation found in single crystals, alternative strategies, such as those based on

Langmuir-Blodgett (L-B) methods, usually result in conjugation defects.[35] Cao and Mallouk have shown that the extent of polymerization of diacetylenic monomers in organometallic crystals depends on the coordinating metal ion; divalent metal ions yield polymers with the greatest extent of conjugation.[10,36] Besides our own work, there has been one prior report of the polymerization of a monolayer prepared from methyl-terminated diacetylene disulfides.[37] Studies such as these have yielded applications for polydiacetylenes as non-linear optical materials,[38,39] semiconductors and photoconductors,[40] drug delivery systems,[41] photolithographic resists,[2,42] and as chemical sensors.[43,44] Finally, there have been several reports of SAMs that can be end-group polymerized using either electrochemical methods or light.[45,46] The utility of these materials may be somewhat limited, however, since the polymers are probably not well ordered and their endgroups are not readily available for synthetic elaboration.

Since our principal interest is in preparing rugged, oriented polydiacetylene mono- and multilayers for optical, electronic, chemical sensing, and lithographic applications, we designed and synthesized three different ω-functionalized diacetylenic *n*-alkanethiols: $HS(CH_2)_{10}C{\equiv}CC{\equiv}C(CH_2)_{10}X$ (X=COOH, DA-COOH; CH_2OH, DA-OH; and CH_3, DA-CH_3). The acid[3,47] and hydroxyl[48] surfaces are

readily amenable to further synthetic elaboration, while the methyl-terminated SAM results in a clean, low-energy surface.

Scheme I illustrates the similarity between the lattice structure of Au-confined, *n*-alkanethiol SAMs (top) and the geometry of unpolymerized and polymerized diacetylene molecules (bottom).[36] The spacing between three-fold hollow sites on the Au(111) surface is 4.99 Å. The organomercaptans that occupy these sites are tilted by about 30-40° with respect to the surface normal and twisted by ~50° (not shown) about the carbon backbone to maximize intermolecular van der Waals interactions.[9] Unlike Langmuir and L-B films, organomercaptans are strongly bound to their supporting surfaces, and therefore are not expected to have the same degree of freedom to alter their conformation to accommodate polymerization. However, as illustrated in Scheme I, the topochemical polymerization geometry is nearly ideal, and little rearrangement should be required to yield linearly polymerized films if the diacetylenic thiols adopt a geometry on Au similar to that of *n*-alkanethiols.

Scheme I

Experimental

Chemicals. Most chemicals required for synthesizing the diacetylenes were of reagent-grade quality, purchased from Aldrich Chemical Co., and used without further purification. Anhydrous sodium hydrogen sulfide was obtained from Alfa Chemical and used

as received. (3-mercaptopropyl)trimethoxysilane was purchased from Hüls America Inc. (Bristol, PA). Water was purified (resistivity ≥ 18 MΩ-cm) using a Milli-Q reagent water system (Millipore).

Synthesis of diacetylenic alkylthiols. The syntheses of DA-COOH and DA-OH were discussed previously.[1] DA-CH_3 was synthesized *via* the same synthetic route using undecylbromide instead of ω-methoxymethoxy alkylbromide (Scheme II).

Scheme II

1-Bromopentacosa-11,13-diyne (**3**). To a stirred solution of **2** (10 mmol in 30 mL of THF) was added n-BuLi (5.9 mL, 1.6 M in hexane) at 0 °C, which was prepared from **1** and undecylbromide in presence of 1.5 M methyl lithium.[1] After 1 h, 1,10-dibromodecane (45 mmol, 13.5g, 5 equiv) was added to the mixture as a solid, followed by addition of 10 mL of HMPA. The reaction mixture was stirred for an additional 30 min at 0 °C. The alkylated product was extracted from the mixture by 2 x 200 mL of petroleum ether. The combined organic layers were washed with 2 x 200 mL of water and dried over anhydrous sodium sulfate. Evaporation of solvent gave the crude product, which was purified by flash column chromatography (silica gel, petroleum ether) to give pure **3** in 23% yield: ^{1}H NMR ($CDCl_3$) δ: 3.400 (2H, t, J = 6.8 Hz), 2.235 (4H, t, J = 6.8 Hz), 1.848 (2H, m), 1.547-1.251 (32H, m), 0.873 (3H, t, J = 6.4 Hz).

1-Mercaptopentacosa-11,13-diyne (**DA-CH_3**). Sodium hydrogen sulfide (NaSH, 0.6 mmol, 6 equiv) was added to a solution

of alkylbromide (**3**, 0.1 mmol) in absolute ethanol (4 mL) and the solution was degassed under Ar for 2 min. The reaction mixture was sonicated for 4-8 h at 50-55 °C, diluted with 3 x 10 mL of CH_2Cl_2, washed with acidic water (2-3 drops of 3 N HCl in 5 mL water), and 2 x 5 mL DI water. The organic layer was dried over anhydrous sodium sulfate and solvent was evaporated to give crude DA-CH_3. The crude mixture was recrystallized in 5 mL of hot hexane and subsequently filtered to give about a 65% yield of purified DA-CH_3 as a slightly yellow solid: ^{1}H NMR ($CDCl_3$) δ: 2.488 (2H, t, J = 7.3 Hz), 2.231 (4H, t, J = 6.7 Hz), 1.561-1.151 (34H, m), 0.872 (3H, t, J = 6.5 Hz).

NMR Spectroscopy. High-field NMR spectra were recorded on a Gemini or XL-200E spectrometer.

FTIR-external reflectance spectroscopy (FTIR-ERS). Substrate preparation for FTIR-ERS experiments was described previously.[2,3] Briefly, about 2000 Å of Au was thermally or e-beam evaporated onto Ti- or Cr-primed (50-100 Å) Si(100) wafers. After dicing into 1.3 x 2.5 cm pieces, the substrates were cleaned in freshly prepared piranha solution (30% H_2O_2:conc. H_2SO_4 = 1:3; **Caution**: piranha solution is a powerful oxidizing agent and reacts violently with organic compounds. It should be discarded immediately after use in a waste container with a loosely fitting lid.) for 15 s, rinsed, and dried. Monolayers were prepared by dipping freshly cleaned substrates into 1 mM THF or $CHCl_3$ solutions of the organomercaptans for 1 h or longer. Following deposition, the modified surfaces were rinsed with solvent and water (additionally, all acid-terminated SAMs were sonicated in 1.0 N

HCl for 5 s and then rinsed with water), and then dried under flowing N_2. Polymerization of the diacetylenic SAMs was performed by placing the substrate into a gas-tight polycarbonate container and irradiating it under a N_2 purge for up to 45 min (but typically 10 min) with a Hg(Ar) pencil-type UV lamp, (Oriel, model 6035 (~1 W)) positioned 0.5 - 1 cm above the substrate.

FTIR-ERS spectra were acquired using a Digilab FTS-40 spectrometer (Bio-Rad, Cambridge, MA) equipped with a Harrick Scientific "Seagull" reflection accessory and a liquid-N_2 cooled MCT detector. All spectra were obtained using *p*-polarized light incident on the substrate at an angle of 84° with respect to the surface normal. All spectra were obtained at 2-cm^{-1} resolution and are the sum of 256 individual spectra. Minimal baseline correction was applied to all spectra.

Raman Spectroscopy. The surface-enhanced Raman spectroscopy (SERS) measurement system was similar to that described previously[3] with a slight modification: instead of the f-250 mm focusing lens, a 10X microscope objective of 0.21 NA (Nikon) was used to focus the incident laser beam. The same objective was also used to collect the scattered Raman photons via a beam-splitting cube (Edmond Scientific, Barrington, NJ). Typical conditions for Raman scattering were 647.1 nm excitation (0.5 mW), 400-mm slit width (equivalent to a 14 cm^{-1} bandpass), and 5 s integration time.

The electrochemical system for roughening Au substrates consisted of a bipotentiostat (model AFRDE5, Pine Instruments, Grove City, PA) which was computer-controlled via a programmable

analog-digital interface board (model AT-MIO-16F-5, National Instruments, Austin, TX). To prepare the roughened Au substrate, a clean Au(111) facet was first obtained by melting and annealing an Au wire (99.9985%, 1.0-mm diameter, Johnson Matthey, Ward Hill, MA) in a H_2/O_2 flame.[22] The facet was then coated with an *n*-hexadecanethiol SAM prepared from a 1 mM ethanol solution. The defect sites within the SAM layer were utilized as nucleation sites on which SERS-active Au particles were electrochemically deposited at 0.3 V (vs. Ag/AgCl, NaCl (3M)) for 30 s from a solution containing 0.1 M $HClO_4$ and 1 mM $HAuCl_4$. To enhance Au particle adhesion, the defect sites were intentionally etched at an electrode potential of 1.1 V prior to Au deposition. SERS-active Au particles prepared by this method can be readily characterized by scanning force microscopy. In this study, a relatively large particle size was chosen (greater than 1 μm) to minimize surface curvature. A detailed discussion of this new type of SERS substrate will be provided in a forthcoming publication.[49] No effort was made to remove the *n*-hexadecanethiol SAM on the Au (111) surface since its surface Raman scattering was below the limit of detection.

Immediately after rinsing with water and ethanol, the roughened Au substrate was immersed in a 1 mM diacetylene monomer solution of $CHCl_3$ for about 10 h, removed, rinsed with ethanol, and dried in a stream of N_2. SERS from the diacetylenic SAM on the Au particles were measured in air. Polymerization under UV irradiation was achieved by placing the substrate 25 cm from a 30-W low-pressure Hg lamp (Conrad-Hanobia, NJ) for 10 min.

UV-vis spectroscopy. Partially transmitting Au substrates for UV-vis measurements were prepared by thermal evaporation of 50 Å of Au onto both sides of (3-mercaptopropyl)trimethoxysilane-primed 1 x 2.5 cm quartz substrates.[3,50,51] The substrates were cleaned using a low-energy Ar plasma (Harrick Scientific Model PD6-32G) for 1 min. SAMs were prepared as described for the FTIR-ERS measurements. The UV-vis spectra (100 scans each, 2-nm resolution) were recorded on a Hewlett-Packard diode-array spectrometer (Model 8452A) by first obtaining a background spectrum of the unpolymerized diacetylenic SAM, and then polymerizing it for various lengths of time without removing the substrate from the spectrometer. The UV light source was maintained 0.5 - 1.0 cm away from the substrate. Throughout these experiments the substrate was kept under a N_2 purge.

Ellipsometry. The substrates used to obtain ellipsometric thickness data were the same as those used for FTIR-ERS analysis. Thickness measurements of the polymerized and unpolymerized diacetylenic SAMs were made using a Gaertner Scientific ellipsometer (Model L116C). The data were obtained using the 488 nm Ar laser line, but the 633 nm He-Ne laser line yielded similar results. A refractive index of 1.46 was assumed for thickness calculations.

Electrochemical Measurements. Substrates for electrochemical measurements were prepared by thermal evaporation of 440 Å of Au onto (3-mercaptopropyl)trimethoxysilane-primed 1.0 x 2.5 cm pieces of glass using methods similar to those discussed for the UV-vis substrates. Au substrates were cleaned for 1 min

in an Ar plasma, and then immediately immersed in a 1 mM THF solution of the diacetylenic thiol for at least 1 day. Prior to polymerization or electrochemical measurements, the substrates were rinsed with THF and water. Diacetylenic SAMs were polymerized identically to those prepared for the FTIR-ERS experiments.

A single-compartment electrochemical cell containing the Au working electrode (immersed electrode area = 0.7 cm^2), a reference electrode (Ag/AgCl, NaCl (3 M)) and a Pt counter electrode, were used to obtain cyclic voltammetric data. Capacitance measurements were carried out in an aqueous 0.1 M KCl electrolyte solution (scan rate = 100 mV/s), and Faradaic electrochemical experiments were performed in a 0.1 M KCl electrolyte solution containing 5 mM $Ru(NH_3)_6Cl_3$ (scan rate = 50 mV/s).

SAM Stability Experiments.

Substrate preparation. Au substrates and SAM films were prepared essentially identically to those used for FTIR-ERS experiments.

Electrochemical desorption. The SAM-modified Au substrates were subjected to cyclic voltammetry in a single-compartment cell configured as described previously. The Au substrate potential was scanned between -0.5 and -1.4 V (vs. Ag/AgCl, NaCl (3 M)) at 50 mV/s in an electrolyte consisting of a 1:1 mixture of 1.0 M aqueous KOH and ethanol using a Pine (Model AFCBP1) potentiostat. Pt gauze was used as a counter electrode. The substrates were scanned for up to 32 cycles and FTIR-ERS

spectra were obtained after 2, 4, 8, 16 and 32 cycles. The magnitude of the absorbance in the IR hydrocarbon stretching region (2800 - 3000 cm^{-1}) was used to determine the extent of reductive stripping of the SAMs.

Thermal processing. The SAM-modified Au substrates were subjected to thermal processing using a tube furnace consisting of a Pyrex glass tube ~0.5 m in length wrapped with heating tape and Al foil. A type K thermocouple was used to measured the temperature of the furnace. To assure effective heat transfer to the SAM, the substrate was contained in a small boat prepared from Al foil. Once the temperature was stabilized at the desired temperature (200 ± 5 °C, unless otherwise stated), the boat containing the modified Au substrate was placed inside the tube for varying lengths of time. Throughout these experiments the tube was under an Ar purge. FTIR-ERS spectra were obtained after cooling in air. SAM stability was evaluated as described for the electrochemical desorption experiments.

Exposure to aggressive solvents. The SAM-modified Au substrates were exposed to a hot (100 °C) base solution, which consisted of a 1:1 mixture of aqueous 1.0 M aqueous KOH and ethanol, contained in a sealed vial for varying lengths of time. FTIR-ERS spectra were obtained after cooling and rinsing the substrates. SAM stability was evaluated as described for the electrochemical desorption experiments.

Results and Discussion

FTIR-ERS. Figure 1 shows FTIR-ERS spectra of a $HS(CH_2)_{10}C{\equiv}CC{\equiv}C(CH_2)_{10}COOH$ SAM before (DA-COOH) and after (PDA-COOH) polymerization by UV light. Prior to polymerization, the DA-COOH spectrum reveals two high-energy absorptions at 2930 cm^{-1} and 2856 cm^{-1} that arise from asymmetric ($\nu_a(CH_2)$) and symmetric ($\nu_s(CH_2)$) methylene stretching modes, respectively (most FTIR-ERS data are summarized in Table 1). The positions of these bands indicate that the hydrocarbon backbones are not structurally ordered as they are in SAMs prepared from *n*-alkanes, which have methylene bands at lower energies ($\nu_a(CH_2)$ = 2918 cm^{-1} and $\nu_s(CH_2)$ = 2851 cm^{-1}).[52] The rigid, rod-like diacetylene groups present in the middle of lattice structure are probably responsible for the decreased packing efficiency of the chains.[53] In addition to the methylene modes, there is also a single, strong absorption at 1719 cm^{-1} arising from the C=O of the carboxylic acid terminal group. The position of this band suggests that the acid groups undergo lateral hydrogen bonding in analogy to acid-terminated alkylthiols.[54,55] The ellipsometrically measured thickness of the DA-COOH SAM is 24 ± 2 Å. Because the length of extended, all-trans DA-COOH is about 32 Å,[56] we infer that alkyl chains are tilted about 42° from the surface normal prior to polymerization.

Figure 1

Table 1

The lower spectrum in Figure 1 reveals the spectral changes attendant upon polymerization of DA-COOH. The PDA-COOH $\nu_a(CH_2)$ band decreases in magnitude by about 30%, shifts to lower energy (2926 cm^{-1}), and sharpens slightly (Δ fwhm = -3 cm^{-1}) which suggest that polymerization causes an orientational change in the alkyl chains and improves their ordering. The $\nu_s(CH_2)$ band also decreases in magnitude, but its position does not change. The position of the C=O band remains unchanged at 1719 cm^{-1}, suggesting that the acid groups remain hydrogen-bonded after polymerization, but the magnitude of the C=O band decreases dramatically after polymerization, which strongly suggests a significant change in end-group orientation.[57] As for the DA-COOH SAM, the measured ellipsometric thickness of the PDA-COOH SAM is about 24 Å. That there is no difference between the thicknesses of the DA and PDA SAMs is the result of a fortuitous cancellation of effects: although the SAMs untilt somewhat after polymerization, the individual molecules that comprise the SAM are actually somewhat shorter following polymerization.[56]

In FTIR-ERS, vibrations are active only if there is a change in the dipole-moment vector component normal to the surface and then the absorbance is proportional to the square of that component dipole-moment change. Spectral differences before and after polymerization are suggestive of molecular reorganization.[58] For the asymmetric and symmetric CH_2 modes to be active, DA-COOH must be both tilted (relative to the surface normal) and twisted (about the alkyl backbone) as shown in Scheme III.[58] A space-filling model of PDA-COOH is shown in Scheme IV.

Scheme III

Scheme IV

After polymerization, we observed that the absorbance of the CH_2 peaks decreases. Since there are no chemical changes in the CH_2 groups during polymerization, the decrease in absorbance must result from the untilting and untwisting of the alkyl chains relative to the initial DA-COOH configuration (bottom panel of Scheme III). A similar argument can be applied to the C=O band at 1719 cm^{-1}. Before polymerization, the C=O group, which has a dipole moment along the C=O bond, is oriented somewhat vertically with respect to the Au surface. After polymerization, the C=O absorbance decreases dramatically implying that the C=O group in PDA-COOH is nearly parallel to the surface.

We were concerned that UV exposure, which is required to polymerize the SAMs, could damage or otherwise change the chemical or structural characteristics of the PDA-COOH SAMs. For example, it has been shown that UV illumination in the presence of air leads to photooxidation of sulfur in *n*-alkanethiols, and renders such SAMs easily removed from the Au substrate.[23,24] To ensure that such destabilization does not occur for PDA-COOH, and that the spectral changes noted above arise only from structural changes attendant upon polymerization, we exposed a SAM composed of mercaptoundecanoic acid (MUA) to UV light under exactly same conditions used to polymerize the DA-COOH SAM. The FTIR-ERS results of this experiment are shown in Figure 2. Before exposure

to UV light, methylene stretching bands are present at $\nu_a(CH_2)$ = 2926 cm^{-1} and $\nu_s(CH_2)$= 2856 cm^{-1},[59] and a strong C=O absorption occurs at 1719 cm^{-1}, as we observed for the DA-COOH and PDA-COOH SAMs. It has been previously noted that the MUA C=O band actually consists of two poorly resolved components at about 1739 and 1718 cm^{-1}, corresponding to nonhydrogen-bonded and laterally hydrogen-bonded acid groups, respectively.[54,55,60] We previously found that when MUA SAMs are rinsed in neutral water the pH is not sufficiently low to yield full protonation; therefore, in this experiment we exposed them (and all other acid-terminated SAMs) to aqueous acid prior to analysis to ensure full protonation. This treatment causes the higher energy C=O band to be replaced by the single peak shown in Figure 2. This effect is fully reproducible.

Figure 2

The important point of these experiments is that under the conditions used here, illumination does not change the MUA SAM: the magnitudes of the peaks, their fwhm, and their positions are identical, within spectral resolution, before and after exposure to UV light. This result contrasts sharply with those reported by Hemminger[23] and Tarlov;[24] however, the experiments reported here were performed in the absence of O_2. This control experiment demonstrates that the conditions used for DA-COOH polymerization do not undermine the structural integrity of the SAMs, and that the spectral changes shown in Figure 1 are associated only with polymerization.

Hydroxyl ($HS(CH_2)_{10}C{\equiv}CC{\equiv}C(CH_2)_{10}OH$)- and methyl ($HS(CH_2)_{10}C{\equiv}CC{\equiv}C(CH_2)_{10}CH_3$)-terminated diacetylene molecules (DA-OH and DA-CH_3, respectively) also yield polymerized SAMs (PDA-OH and PDA-CH_3, respectively) upon exposure to UV light. FTIR-ERS spectra of DA-OH and PDA-OH SAMs are shown in Figure 3. The $\nu_a(CH_2)$ and $\nu_s(CH_2)$ bands are present at 2927 cm^{-1} and 2856 cm^{-1}, respectively, but upon polymerization these bands decrease in intensity by about 25% and their positions are unchanged. The ν(OH) band centered around 3300 cm^{-1} is broad and poorly defined before and after polymerization. These results are in general agreement with the DA-COOH/PDA-COOH system discussed earlier, and they suggest that the DA-COOH SAM undergoes a small but significant structural change upon polymerization. To ensure that UV illumination does not destabilize the PDA-OH SAM, we performed a control experiment analogous to the MUA experiment discussed earlier (Figure 4). The results indicate that SAMs prepared from 11-mercaptoundecanol (MUD) do not undergo significant spectral changes upon UV irradiation.

Figure 3

Figure 4

FTIR-ERS data for SAMs prepared from the methyl-terminated diacetylene are shown in Figure 5. Prior to polymerization, the spectrum of DA-CH_3 reveals $\nu_a(CH_2)$ and $\nu_s(CH_2)$ bands at 2927 cm^{-1} and 2857 cm^{-1}, respectively, and the $\nu_a(CH_3)$ band is present at 2962 cm^{-1}. Upon polymerization, the bands do not shift but their

magnitude decreases by about 15%, indicating they undergo small but significant structural changes upon polymerization.

Figure 5

Raman spectroscopy. Figure 6 shows the SERS spectra of polymerized SAMs of DA-COOH, DA-OH, and DA-CH_3 on roughened Au surfaces after UV irradiation. The resemblance of the three spectra is not surprising since their principal bands originate from vibrations of the PDA backbone, which contains conjugated and alternating C=C and C≡C bonds.[3] Lewis and Batchelder have analyzed the normal modes of several PDAs based on bulk Raman spectra using a simplified model containing only five independent force constants.[61,62] According to this model, the peaks around 1444 cm^{-1} and 2075 cm^{-1} can be assigned to the C=C and C≡C stretching vibrations, respectively. Because of the extensive electronic delocalization in the PDA backbone these frequencies are lower than those for isolated C=C and C≡C bonds (1620 cm^{-1} and 2260 cm^{-1}, respectively).[63,64] The remaining prominent peak around 687 cm^{-1} is due to an in-plane bending mode of the backbone, but this assignment is less definitive due to its low frequency and the uncertainty of the force constants used in the Lewis-Batchelder model.

Figure 6

The peak positions of the C=C and C≡C stretching vibrations agree with those observed in previous studies.[3,37,65,66] For example, Batchelder et al. detected two bands at 1455 cm^{-1} and 2074 cm^{-1} from the polymerized SAM of a DA-CH_3 derivative on smooth Au.[37] Chen et al. reported SERS at 1456 cm^{-1} and 2078 cm^{-1} from the polymerized L-B film of a similar DA derivative on Ag island films.[65] These peak positions suggest, and UV-vis spectroscopic data discussed in the next section confirm, that the polymerized DA films exist in a structurally ordered "blue" phase.[62] In contrast, the less ordered "red" phase would show bands around 1517 cm^{-1} and 2115 cm^{-1} according to a previous study on L-B films of PDA.[66] We have observed a weak band around 2135 cm^{-1}, which may indicate the presence of a small fraction of the red phase. However, this peak should be accompanied by the one around 1517 cm^{-1}, which is assigned to the C=C stretching mode of the red phase, and it is not.

Besides low-power, UV-induced polymerization, a DA monolayer can also be polymerized by the incident laser light at 647.1 nm. This result agrees with those of Batchelder et al. who observed that a He-Ne laser at 632.8 nm initiated polymerization,[37] and of Angkaew et al. who observed similar phenomenon using a 750.7 nm titanium-sapphire laser.[63] We found that the rate of laser-induced polymerization increases as the laser power density increases. With the present experimental setup, a large power density is produced by focusing the laser beam with the 10X microscope objective. As a result, the polymerization can be initiated with a power as low as 0.2 mW. SERS spectra of laser-induced PDA

monolayers are very similar to those obtained after UV irradiation except for a subtle difference: the peak due to the C≡C stretching vibration, which occurs at 2075 cm^{-1} after UV-induced polymerization, is located 2-6 cm^{-1} lower when polymerization is laser induced. This may be explained by the strain theory of Batchelder et al. who concluded that the C≡C stretching frequency decreases as the internal crystal strain increases.[62,67] Since laser-induced polymerization is likely to be incomplete, a higher crystal strain within the two dimensional monolayer lattice is expected, which leads to a lower C≡C stretching frequency.[62] In contrast, the fractional conversion from DA to PDA after UV irradiation should be higher than that without UV irradiation, resulting in lower strain and higher stretching frequency. The internal strain is relaxed completely when all the DA is converted to PDA.

No SERS from an unpolymerized DA monolayer can be detected. The failure to detect the C≡C bonds in the DA monolayer may be attributed to the large distance between these bonds and the Au surface.[68] It is surprising, however, that we did not detect SERS from the C-S stretching vibration which is closer to surface and which has been observed previously.[69] We do not fully understand this observation other than noting that the surface morphology of our roughened Au substrate and our collection optics may not have been sufficiently well optimized to detect this band or others resulting from vibrations of the methylene skeleton. In comparison, detection of the PDA backbone is possible because of the additional resonance enhancement. As we discuss in the next

section, the blue form of PDA has an intense absorption band near 620 nm (Figures 7 and 8), a band that encompasses the 647.1 nm laser line. The resonance enhancement mechanism is well supported by many previous studies of Raman scattering from PDA single crystals, which showed that the Raman excitation profile follows closely the absorption profile.[62]

UV-vis spectroscopy. Upon polymerization, diacetylenic SAMs absorb visible light. The optical properties of single crystals of PDA have been extensively studied.[70] The carbon backbone of a fully conjugated PDA is planar and the lowest energy optical transition (π - π^*) is typically located at about 620 nm. Therefore, fully conjugated PDA absorbs red light and appears as a blue polymer. However, distortion of the conjugated carbon backbone due to disorder or strain reduces the extent of orbital overlap and shortens the average conjugation length. This shifts the π - π^* transition to a higher energy (~540 nm), and causes the polymer to appear red. Day and Ringsdorf[34] reported a blue to red shift in the PDA absorption spectrum when they irradiated crystalline PDA with UV light for an extended period of time. The authors attributed this shift to a re-orientation of the carbon backbone of the blue polymer, which effectively reduces the conjugation length, increases the energy of the optical transition, and changes the polymer from blue to red.

Tieke and Lieser[71] studied the polymerization of L-B films of diacetylenes having the general formula $CH_3(CH_2)_{m-1}C{\equiv}CC{\equiv}C(CH_2)_nCOOH$. The color of the PDA L-B films depends on the packing of the monomers. For well-packed films

(m=12, n=8; m=10, n=8), the polymer is blue indicating a high level of conjugation, but after extensive illumination it converts to the red polymer like the solid-state materials. For the less well-packed films (m=16, n=2; m=16, n=0), only the red polymer obtains.

We exposed SAMs prepared from DA-COOH and DA-OH to UV light for varying lengths of time and measured the resulting optical spectra in the range 400-800 nm. The spectra at the top of Figure 7 show the spectral evolution of a DA/PDA-COOH SAM over a period of 13 min. After illuminating with UV light for 3 min, a very weak, broad absorbance having a wavelength maximum (λ_{max}) in the range 620-650 is apparent. As shown at the bottom of Figure 7, polymerization is complete after about 13 min, at which time there is a fairly well-developed peak present at 620 nm. Based on previous results obtained from DA/PDA crystals and L-B films, and the discussion in the previous section, we infer that there is a relatively high level of conjugation in the PDA SAMs. In contrast to results from PDAs in the solid state and in L-B films, the PDA SAMs do not change into the red polymer even after extended UV illumination. We believe the conjugation stability of the PDA SAMs results from its strong interaction with the Au surface, which tends to reduce structural flexibility and impede re-orientation after polymerization.

Figure 7

Figure 8 shows analogous spectral data for a DA/PDA-OH SAM. The results are strikingly similar to those shown for the DA/PDA-COOH SAM in Figure 7. For example, λ_{max} is present around 620 nm, and the polymer remains blue even after extended UV illumination. The only notable difference between the acid- and hydroxyl-terminated materials is that the latter polymerizes somewhat more quickly: no change in the absorbance at λ_{max} is observed after 7 min.

Figure 8

Electrochemical Methods. Electrochemical methods have often been used as a convenient and highly sensitive means for examining the packing quality and number of defects within SAMs.[52,72] There are two electrochemical approaches for evaluating the mass-transfer inhibiting properties of SAMs: the first is based on capacitive measurements and the second on Faradaic processes.

When an electrochemical interface is approximated as a parallel plate capacitor, its capacitance per unit area (C) is given by eq 2, where ε is the dielectric constant of the film,

$$C=\varepsilon\varepsilon_0/d_{eff} \qquad (2)$$

ε_0 is the permittivity of free space, and d_{eff} is the effective thickness of the SAM.[73,74] For an impermeable mass-transfer barrier, d_{eff} is simply the thickness of the SAM (bottom of Scheme

V). However, if ions are able to penetrate through the SAM (top of Scheme V), then d_{eff} is reduced and C increases. Thus, the magnitude of C, which is easily measured by cyclic voltammetry,[74] is a measure of the extent to which the electrolyte penetrates the SAM. There is one potential complication to this approach when it is used for comparing diacetylenic SAMs before and after polymerization. If the length of the polymer changes as a result of polymerization, then d_{eff} will change and the correlation between changes in capacitive current and defect density will be compromised. However, as discussed earlier, the thicknesses of the diacetylenic SAMs used here are unaffected by polymerization.

Scheme V

Figure 9 illustrates the results of the capacitive approach for evaluating the barrier properties of hydroxyl- and acid-terminated SAMs before and after polymerization.[73] The voltammograms were obtained in a potential region where little Faradaic current flows, and the capacitive current was measured in the region around 0 V where Faradaic processes are minimal and the current is not potential dependent. The measured double-layer capacitance of DA-OH is 4.9 $\mu F/cm^2$, which is substantially higher than the capacitance of a much shorter hydroxyl-terminated *n*-alkanethiol SAM comprised of $HS(CH_2)_{10}CH_2OH$ (<2 $\mu F/cm^2$).[73] This result almost certainly reflects structural deficiencies in DA-OH SAMs. The capacitance of the DA-OH SAM decreases monotonically until polymerization is complete and the capacitance reaches a

constant minimum value of 2.2 $\mu F/cm^2$. The important point is that PDA-OH is a significantly better mass transfer barrier than DA-OH, which implies that photopolymerization actually serves to improve the structural and barrier properties of the monolayer. We speculate that the principal reason for this observation is that the dimensions of defects within DA SAMs are dynamic and while their average size is fixed, the standard deviation of the pore size is fairly large which leads to significant ion penetration of the film. Following polymerization, however, the films are much more rigid[4] and while the average pore size may not decrease, the time-dependent variation is smaller which leads to a reduction in the average depth of ion penetration.

Figure 9

The capacitance of the DA-COOH SAM (1.3 $\mu F/cm^2$) is substantially lower than the DA-OH SAM, and is approximately the same as for the $HS(CH_2)_{10}COOH$ (~3 $\mu F/cm^2$) after correcting for differences in d_{eff}.[73] Following 10 min of illumination the capacitance of the DA-COOH SAM decreased to 0.8 $\mu F/cm^2$, which is as low as a very good methyl-terminated SAM.[73] As observed for the DA-OH/PDA-OH system, the capacitance decreases monotonically as a function of illumination time until the SAM is fully polymerized. As discussed earlier, the lower capacitance reflects a decrease in ion penetrability arising from film stiffening and possibly increased ordering. Since the DA-OH and DA-COOH molecules are the same except for their endgroup functionality, we speculate that

the large differences between the capacitances of the acid- and hydroxy-terminated SAMs reflects differences in endgroup structure perhaps resulting from intramonolayer hydrogen bonding.

In addition to capacitive measurements, it is also possible to evaluate defects within SAMs using Faradaic electrochemistry. In this experiment, a SAM-coated Au substrate is immersed in an electrolyte solution containing redox-active probe molecules. Depending on the size and chemical nature of the probe molecules and the nanoscopic structure of the SAM, the probe molecules may completely or partially penetrate the SAM and undergo electron transfer with the Au substrate. Three possible modes of interaction are possible. First, if there are many defects within the SAM that permit probe molecules to exchange electrons with the underlying substrate, then the resulting cyclic voltammetric response will appear peak-shaped.[52,72] This is a consequence of linear diffusion of the probe molecule to the substrate. Second, if there is a low density of micron- or nanometer-scale defects, then each defect will behave as a single ultramicroelectrode.[72,75,76] Diffusion to individual electrodes will be radial, and as long as they are spaced sufficiently far apart that their diffusion layers do not overlap, the resulting cyclic voltammetric response will appear plateau shaped at potentials much past $E^{o'}$.[72] Third, if there are no defect sites through which probe molecules can completely or partially penetrate, their average point of closest approach to the electrode will be roughly defined by the average thickness of the monolayer.[77-79] In this case it may be possible to observe very

small tunneling currents between the substrate and probe, which will result in cyclic voltammograms characterized by an exponential increase in current.

Interpretation of results from cyclic voltammetric experiments is most straightforward for SAMs that contain monodispersed nanometer- to micron-scale defects that are regularly spaced and sufficiently far apart that their diffusion layers do not overlap. In this case it is sometimes possible to determine detailed structural information about defects such as their number density and size; however, this situation is never realized experimentally. Interpretation is further complicated because the cyclic voltammetric response depends on the size, shape, and charge of the solution-phase probe molecule.[72] Thus, electrochemical methods are best used for *comparing* the average properties of SAMs or other thin films, rather than attempting to determine absolute defect configurations.

The cyclic voltammetric data shown in Figure 10 were obtained using exactly the same SAM-modified electrodes that were used for the capacitance measurements described earlier. For these experiments the aqueous electrolyte solution contained 5 mM $Ru(NH_3)_6^{3+}$ and 0.1 M KCl. Comparing first the relative penetrability of the hydroxyl- and acid-terminated SAMs, we find that the results mirror those obtained from the capacitance measurements: the hydroxyl-terminated SAMs are more permeable than the acid-terminated monolayers. We also find that there is a substantial decrease in probe penetration upon polymerization for both the DA-OH/PDA-OH and DA-COOH/PDA-COOH systems. Based on

these results, the PDA-COOH SAM resists $Ru(NH_3)_6^{3+}$ mass transfer at least as well as a typical methyl-terminated *n*-alkanethiol SAMs.[72]

Figure 10

Durability of PDA Films

Although we discussed several important applications of diacetylenic SAMs in the introduction, their principal virtue is that they are more durable than SAMs prepared from *n*-alkanethiols since the PDA SAMs are polypodal and have much higher molecular weights. We have already demonstrated that the DA SAMs have many of the same structural characteristics of their *n*-alkanethiol analogs, which suggests they could be seamless replacements for them if their enhanced durability compensates their more challenging synthesis.[1] In this section we show that acid-terminated PDA SAMs are indeed far more durable than *n*-alkanethiols as judged by their enhanced stability under a variety of harsh conditions. We chose to evaluate the acid-terminated SAMs, rather than PDA-CH_3, since the former is more synthetically flexible.[47,80] Undoubtedly PDA-CH_3 is even more durable than the acid-terminated material. We have chosen to evaluate the electrochemical and thermal stability of the PDA SAMs, and their resistance to aggressive solvents since these are environments in which SAMs are likely to find technologically significant applications.

Electrochemical desorption. SAMs may find applications as corrosion inhibitors and as chemically sensitive interfaces for

electrochemical-based sensors. However, Porter and coworkers have shown that the stability of SAMs prepared from *n*-alkanethiols are unstable outside of a fairly narrow range of substrate potentials.[20,21] Their results showed oxidative and reductive desorption occur at about +0.8 V and -0.8 V (vs. Ag/AgCl, satd KCl), respectively, in aqueous 0.5 M KOH. The exact desorption potential depends on the electrolyte solution, substrate, scan rate, and the thickness of the SAM.[20,21] Nearly all of the monolayer desorbs from the surface after two voltammetric scans. In a related study, Schneider and Buttry showed that *n*-alkanethiols can be reductively desorbed in acetonitrile and dimethylformamide.[17]

We compared the stability of SAMs prepared from *n*-hexadecanethiol ($HS(CH_2)_{15}CH_3$, HDT), DA-COOH, and PDA-COOH by scanning the potential of a monolayer-coated electrode between -0.5 and -1.4 V (vs. Ag/AgCl (3 M NaCl)) at 50 mV/s in an electrolyte consisting of a 1:1 mixture of 1.0 M aqueous KOH and ethanol. These conditions are more aggressive than those used by Porter et al.[20,21] We evaluated the extent of SAM desorption by examining the electrodes by FTIR-ERS after 0, 2, and 16 cyclic voltammetric scans (Figure 11). Spectroscopic analysis is more quantitative for a broader range of surface coverages than the electrochemical methods described earlier in this paper.[72,81]

Figure 11

Prior to electrochemical stripping, the spectrum of the HDT-modified Au substrate shows absorbances at 2965 and 2879 cm^{-1} for the methyl stretching modes and 2919 and 2851 cm^{-1} for the methylene stretching modes, which are in accord in with previous results.[52] After 2 cyclic voltammetric scans the peak at 2878 cm^{-1} disappears completely, and the peaks at 2965 and 2851 cm^{-1} decrease significantly. The peak at 2919 cm^{-1} shifts to 2911 cm^{-1} and also decreases. This result indicates that most of the HDT is stripped from the Au substrate after just 2 scans in accord with previous reports.[20,21] The intensity of the HDT hydrocarbon bands decreases continuously until, after 16 voltammetric scans, only a very small peak at 2911 cm^{-1} remains. The material that gives rise to this band may be residual HDT but is more likely adventitious hydrocarbon material that adsorbs to the Au surface during transfer from the electrochemical cell to the spectrometer. Additional scans did not reduce the intensity of these peaks further (Figure 12).

Figure 12

Results similar to those obtained for HDT were obtained for unpolymerized DA-COOH (Figures 11 and 12), indicating that their level of stability is similar. After polymerization, however, the PDA-COOH SAM shows considerably enhanced stability. As shown in Figure 11, there is no discernible diminution of the hydrocarbon stretching peaks after 16 scans. Even after 32 scans (Figure 12) the PDA-COOH monolayer remains intact, at least as measured by

FTIR-ERS. We attribute this result to the fact that PDA-COOH is a macromolecule with attendant high molecular weight, low solubility,[17] and many points of surface attachment per molecule. Some of these attachment points might not survive the potential excursions, but clearly some of them do. Figure 12 summarizes the dramatic results of this important experiment. We also subjected a PDA-CH_3 SAM to the same electrochemical conditions used for the PDA-COOH experiment and obtained essentially identical results as shown at the bottom of Figure 5 (spectrum EC-32).

Thermal processing. Organomercaptan SAMs have been used as resists for lithographic applications.[19,22-28] In some cases, such as those involving chemical vapor deposition (CVD), high processing temperatures are required. Other applications such as corrosion inhibition, chemical sensing, adhesion, and lubrication might also involve elevated temperatures.

It has been shown that shorter ($\leq$ 10 carbon atoms) *n*-alkanethiol SAMs are thermally stable in vacuum up to about 100 °C, but that even at this temperature there are surface-phase transitions that lead to decreased packing density and attendant loss in SAM barrier properties.[82,83] For example, Results from scanning tunneling microscopy reported by Poirier et al.[82] showed that the surface adlayer structure of *n*-octanethiol and *n*-decanethiol SAMs changed from close-packed c(4 x 2) to the more open p x $\sqrt{3}$ phase when annealed at 100 °C in ultrahigh vacuum (UHV), and heating to 300 °C leads to monolayer desorption. Scoles et al.[83] confirmed these results using x-ray and He diffraction methods by annealing in the temperature range 80 - 135

°C in UHV. However, heating to 200 °C resulted in complete desorption of the monolayer from the surface. McCarley et al, showed that at temperatures less than 100 °C, long-chain SAMs are relatively stable for up to 1 h.[84] Our own results show that under technologically relevant conditions, for example in the presence of a CVD precursor at atmospheric pressure, the temperature range over which *n*-alkanethiol SAMs are stable is likely to be reduced.[19]

We heated SAMs prepared from HDT, DA-COOH, and PDA-COOH to 200 °C for varying lengths of time in an Ar-purged tube furnace and then evaluated the extent of SAM desorption using FTIR-ERS. Figure 13 shows the results of this experiment. Before heating the HDT monolayer has characteristic bands attributable to methyl and methylene modes at the same energies given in the previous section (Figure 11). After heating at 200 °C for only 2 min the spectrum of the HDT SAM changes: the peak at 2879 cm^{-1} disappears, while the peaks at 2965, 2919 and 2851 cm^{-1} shift to 2961, 2924 and 2855 cm^{-1}, respectively. Moreover, the absorbance of the peaks at 2924 and 2855 cm^{-1} becomes larger while that of the peak at 2961 cm^{-1} is attenuated. From these data we conclude that these conditions lead to a dramatic change in the average molecular orientation of HDT and possibly some desorption.[58] After heating for 5 min at 200 °C, all the IR peaks disappear implying complete desorption of HDT.

Figure 13

Prior to heating, the DA-COOH SAM has characteristic methylene stretching modes at 2930 and 2856 cm^{-1} (Figure 13). Upon thermal treatment at 200 °C the absorbance of these bands decrease by about 60%, but even after 5 min they do not disappear completely as they do for HDT SAMs. This may suggest partial thermal polymerization.[62,67] In contrast to this result, the PDA-COOH methylene peak intensities decrease by only about 15% after the first 2 min of heating. This small change in IR absorbance could easily result from a slight thermally driven structural rearrangement of the hydrocarbon chains,[58] or it may reflect desorption of DA-COOH present in the PDA film as a result of incomplete polymerization. After the initial decrease in peak intensity at 2 min, there is no further decrease even after 1 h of additional heating at 200 °C. Only after raising the substrate temperature to 300 °C does the PDA-COOH SAM finally desorb. From these results we conclude that the polymerized monolayer is substantially more thermally stable than simple *n*-alkanethiol SAMs, probably for the reasons discussed in the preceding section.

Exposure to aggressive solvents. Simple *n*-alkanethiols are quite stable in neutral, aqueous solvents at room temperature, presumably because of the poor solubility of these materials in water. However, in many organic solvents,[17,85] at extreme pHs, or at elevated solvent temperature unpolymerized SAMs are prone to desorption. This is a particularly troublesome characteristic for many technological applications of SAMs, including lubrication, adhesion, and lithography.

To compare the durability of unpolymerized and polymerized SAMs, we exposed HDT and PDA-COOH to an especially aggressive solvent: a 1:1 mixture of ethanol and 1.0 M aqueous KOH at 100 °C, and then evaluated the effects using FTIR-ERS. Figure 14 illustrates the results of this experiment. Prior to exposure, the HDT SAM has the hydrocarbon IR fingerprint discussed in the two previous sections. After exposure to the hot, basic solvent for 2 min essentially the entire SAM desorbs. In contrast to this result, however, there is little change in the FTIR-ERS spectrum of the PDA-COOH modified substrate after solvent exposure. These results underscore the enhanced stability of the PDA SAMs.

Figure 14

Summary and Conclusions

Here, we have addressed two major issues: (1) detailed characterization of monomeric and polymerized diacetylenic alkylthiols having three different endgroups, and (2) comparison of the relative stability of *n*-alkanethiols and unpolymerized and polymerized diacetylenic alkylthiols. The results indicate that all three DAs self assemble onto gold substrates to yield organized monolayers and undergo subsequent topochemical polymerization upon exposure to UV light. Moreover, the polymerized materials are far more dimensionally stable than either the unpolymerized DAs or simple *n*-alkanethiols. Given the fragility of the latter two materials, we believe they are, in

contrast to the PDAs, generally unsuitable for most technological applications.

At the present time, we are exploring additional mechanical and structural aspects of the PDAs with a view towards understanding their visco-elastic properties and the length of the individual oligomeric chains. We have also begun to integrate these materials into chemically sensitive interfaces[80] and are evaluating their adhesive properties.[5]

Acknowledgments

R.M.C. and K.C.C. gratefully acknowledge financial support from the National Science Foundation (CHE-9313441) and the Office of Naval Research. This work was also funded in part under contract from Sandia National Laboratories, supported by the U. S. Department of Energy under contract No. DE-AC04-94AL85000. T. K. acknowledges financial support from the Hallym Academy of Sciences, Hallym University. L.S. and Q.Y. acknowledge financial support from the University of Minnesota in the form of start-up funds and a summer fellowship. R.M.C. thanks Prof. Marcetta Darensbourg for use of the UV-vis spectrometer, and L.S. thanks Prof. Kent Mann for the use of the low-pressure Hg lamp.

References and Notes

(1) Kim, T.; Crooks, R. M. *Tetrahedron Lett.* **1994**, *35*, 9501.

(2) Chan, K. C.; Kim, T.; Schoer, J. K.; Crooks, R. M. *J. Am. Chem. Soc.* **1995**, *117*, 5877.

(3) Kim, T.; Crooks, R. M.; Tsen, M.; Sun, L. *J. Am. Chem. Soc.* **1995**, *117*, 3963.

(4) Shinn, N.; Ricco, A. J.; Kim, T.; Crooks, R. M., Sandia National Laboratories and Texas A&M University, unpublished results.

(5) Houston, J. E.; Crooks, R. M., Sandia National Laboratories and Texas A&M University, unpublished results.

(6) Thomas, R. C.; Houston, J. E.; Michalske, T. A.; Crooks, R. M. *Science* **1993**, *259*, 1883.

(7) Thomas, R. C.; Kim, T.; Crooks, R. M.; Houston, J. E.; Michalske, T. A. *J. Am. Chem. Soc.* **1995**, *117*, 3830.

(8) Bigelow, W. C.; Pickett, D. L.; Zisman, W. A. *J. Colloid Sci.* **1946**, *1*, 513.

(9) Dubois, L. H.; Nuzzo, R. G. *Annu. Rev. Phys. Chem.* **1992**, *43*, 437, and references therein.

(10) Cao, G.; Hong, H.; Mallouk, T. E. *Acc. Chem. Res.* **1992**, *25*, 420.

(11) Ulman, A. *Introduction to Ultrathin Organic Films from Langmuir Blodgett to Self-Assembly*; Academic Press: New York, 1991.

(12) Chailapakul, O.; Sun, L.; Xu, C.; Crooks, R. M. *J. Am. Chem. Soc.* **1993**, *115*, 12459.

(13) Nuzzo, R. G.; Allara, D. L. *J. Am. Chem. Soc.* **1983**, *105*, 4481.

(14) Sun, L.; Crooks, R. M. *Langmuir* **1993**, *9*, 1951.

(15) Poirier, G. E.; Tarlov, M. J. *Langmuir* **1994**, *10*, 2853.

(16) Crooks, R. M. Texas A&M University, unpublished results.

(17) Schneider, T. W.; Buttry, D. A. *J. Am. Chem. Soc.* **1993**, *115*, 12391.

(18) Chidsey, C. E. D.; Bertozzi, C. R.; Putvinski, T. M.; Mujsce, A. M. *J. Am. Chem. Soc.* **1990**, *112*, 4301.

(19) Schoer, J. K.; Ross, C. B.; Crooks, R. M.; Corbitt, T. S.; Hampden-Smith, M. J. *Langmuir* **1994**, *10*, 3319.

(20) Widrig, C. A.; Chung, C.; Porter, M. D. *J. Electroanal. Chem.* **1991**, *310*, 335.

(21) Walczak, M. M.; Popenoe, D. D.; Deinhammer, R. S.; Lamp, B. D.; Chung, C.; Porter, M. D. *Langmuir* **1991**, *7*, 2687.

(22) Ross, C. B.; Sun, L.; Crooks, R. M. *Langmuir* **1993**, *9*, 632.

(23) Huang, J. Y.; Hemminger, J. C. *J. Am. Chem. Soc.* **1993**, *115*, 3342.

(24) Tarlov, M. J.; Burgess, D. R. F.; Gillen, G. *J. Am. Chem. Soc.* **1993**, *115*, 5305.

(25) Kumar, A.; Whitesides, G. M. *Science* **1994**, *263*, 60.

(26) Lopez, G. P.; Biebuyck, H. A.; Whitesides, G. M.; Frisbie, C. D. *Science* **1993**, *260*, 647.

(27) Tiberio, R. C.; Craighead, H. G.; Lercel, M.; Lau, T.; Sheen, C. W.; Allara, D. L. *Appl. Phys. Lett.* **1993**, *62*, 476.

(28) Kumar, A.; Biebuyck, H. A.; Abbott, N. L.; Whitesides, G. M. *J. Am. Chem. Soc.* **1992**, *114*, 9188.

(29) Kepley, L. J.; Crooks, R. M.; Ricco, A. J. *Anal. Chem.* **1992**, *64*, 3191, and references therein.

(30) Li, Y.; Chailapakul, O.; Crooks, R. M. *J. Vac. Sci. Technol. B.* **1995**, *13*, 1300.

(31) Tangyunyong, P.; Thomas, R. C.; Houston, J. E.; Michalske, T. A.; Crooks, R. M.; Howard, A. J. *Phys. Rev. Lett.* **1993**, *71*, 3319.

(32) Wegner, G. Z. *Naturforsch.* **1969**, *24b*, 824.

(33) Lando, J. B. In *Polydiacetylenes*; Bloor, D. and Chance, R., Eds.; Nijhoff: Dordrecht, The Netherlands, 1985.

(34) Day, D. R.; Ringsdorf, H. *Makromol. Chem.* **1979**, *180*, 1059.

(35) Wilson, T. E.; Ogletree, D. F.; Salmeron, M. B.; Bednarski, M. D. *Langmuir* **1992**, *8*, 2588, and references therein.

(36) Cao, G.; Mallouk, T. E. *J. Solid State Chem.* **1991**, *94*, 59.

(37) Batchelder, D. N.; Evans, S. D.; Freeman, T. L.; Haussling, L.; Ringsdorf, H.; Wolf, H. *J. Am. Chem. Soc.* **1994**, *116*, 1050.

(38) Axon, T. L.; Bloor, D.; Molyneux, S.; Kar, A. K.; Wherrett, B. S. *Proc. SPIE* **1993**, *2025*, 374.

(39) Winful, H. G.; Hartburger, J. H.; Garmire, E. *Appl. Phys. Lett.* **1979**, *35*, 379.

(40) Day, D. R.; Lando, J. B. *J. Appl. Polym. Sci.* **1981**, *26*, 1605.

(41) Koch, H.; Ringsdorf, H. *Makromol. Chem.* **1981**, *182*, 255.

(42) Niederwald, H.; Seidel, H.; Güttler, W.; Schwoerer, M. *J. Phys. Chem.* **1984**, *88*, 1933.

(43) Reichert, A.; Nagy, J. O.; Spevak, W.; Charych, D. *J. Am. Chem. Soc.* **1995**, *117*, 829

(44) Berman, A.; Ahn, D. J.; Lio, A.; Salmeron, M.; Reichert, A.; Charych, D. H. *Science* **1995**, *269*, 515.

(45) McCarley, R. L.; Willicut, R. J. *J. Am. Chem. Soc.* **1994**, *116*, 10823.

(46) Ford, J. F.; Vickers, T. J.; Mann, C. K.; Schlenoff, J. B. *Langmuir*, **1996**, *12*, 1944.

(47) Duevel, R. V.; Corn, R. M. *Anal. Chem.* **1992**, 337.

(48) Sun, L.; Thomas, R. C.; Crooks, R. M.; Ricco, A. J. *J. Am. Chem. Soc.* **1991**, *113*, 8550.

(49) Tong, X.; Sun, L., University of Minnesota, manuscript in preparation.

(50) Goss, C. A.; Charych, D. H.; Majda, M. *Anal. Chem.* **1991**, *63*, 85.

(51) DiMilla, P. A.; Folkers, J. P.; Biebuyck, H. A.; Haerter, R.; Lopez, G. P.; Whitesides, G. M. *J. Am. Chem. Soc.* **1994**, *116*, 2225.

(52) Porter, M. D.; Bright, T. B.; Allara, D. L. Chidsey, C. E. D. *J. Am. Chem. Soc.* **1987**, *109*, 3559.

(53) Evans, S. D.; Urankar, E.; Ulman, A.; Ferris, N. *J. Am. Chem. Soc.* **1991**, *113*, 4121.

(54) Sun, L.; Crooks, R. M.; Ricco, A. J. *Langmuir* **1993**, *9*, 1775

(55) Sun, L.; Kepley, L. J.;Crooks, R. M.; *Langmuir* **1992**, *8*, 2101

(56) In ref. 3 we estimated the length of DA-COOH and PDA-COOH molecules to be 30 Å and 28 Å, respectively, but using computer modeling methods (InsightII, Biosym), we have refined these values slightly. The correct lengths of the DA-COOH and PDA-COOH molecules are 32 Å and 30 Å, respectively.

(57) Wilson, Jr., E. B.; Decius, J. C.; Cross, P. C. *Molecular Vibrations*; Dover: New York, 1955; p 43.

(58) Nuzzo, R. G.; Dubois, L. H.; Allara, D. L. *J. Am. Chem. Soc.* **1990**, *112*, 558.

(59) The $\nu_a(CH_2)$ and $\nu_s(CH_2)$ energies are both about 6 cm^{-1} higher than we reported previously for MUA (see ref. 54, 55, and 60). This apparent discrepency arises from a structural change that occurs during aging of the films. In previous studies we always measured the IR spectrum immediately after forming the SAM, but all the acid-terminated films discussed

here were aged for periods of up to 2 days prior to spectral aquisition. The shift in the methylene bands in the acid-terminated SAMs (only) upon aging is a fully reproducible effect, and probably reflects relaxation of the hydrocarbon chains.

(60) Yang, H. C.; Dermody, D. L.; Xu, C.; Ricco, A. J.; Crooks, R. M. *Langmuir* **1996**, *12*, 726.

(61) Bloor, D.; Preston, F. H.; Ando, D. J.; Batchelder, D. N. in *Structural Studies of Macromolecules by Spectroscopic Method*; Iven, K. J. Ed.; John Wiley & Sons: London, 1976; Chap. 8.

(62) Batchelder, D. N.; Bloor, D. in *Advances in Infrared and Raman Spectroscopy*; Clark, R. J. H., Hester, R. E., Eds.; Wiley Heyden: London, 1984; pp. 133-209.

(63) Angkaew, S.; Wang, H. -Y.; Lando, J. B. *Chem. Mater.* **1994**, *6*, 1444.

(64) Lin-Vien, D.; Colthup, N. B.; Fateley, W. G.; Grasselli, J. G. in *The Handbook of Infrared and Raman Characteristic Frequencies of Organic Molecules*; Academic Press: San Diego, 1991.

(65) Chen, Y. J.; Carter, G. M. and Tripathy, S. K. *Solid State Comm.* **1985**, *54*, 19.

(66) Burzynski, R.; Prasad, P. N.; Biegajski, J.; Cadenhead, D. A. *Macromolecules* **1986**, *19*, 1059.

(67) Bloor, D.; Dennedy, R. J.; Batchelder, D. N. *J. Polym. Sci.: Polym. Phys. Ed.* **1979**, *17*, 1355-1366.

(68) Tsen, M.; Sun, L. *Anal. Chim. Acta.* **1995**, *307*, 333-340.

(69) Bryant, M. A.; Pemberton, J. E. *J. Am. Chem. Soc.* **1991**, *113*, 8284.

(70) Kuriyama K.; Kikuchi H.; and Kajiyama T. *Langmuir* **1996**, *12*, 2283.

(71) Tieke, B.; Lieser, G.; *J. Colloid Interface Sci.* **88**, *2*, 471.

(72) Chailapakul, O.; Crooks, R. M. *Langmuir* **1993**, *9*, 884.

(73) Chidsey, C. E. D.; Loiacono, D. N. *Langmuir*, **1990**, *6*, 682.

(74) Bard, A. J.; Faulkner, L. R. *Electrochemical Methods*; Wiley: New York, 1980; pp 10-14.

(75) Sabatani, E.; Rubinstein, I. *J. Phys. Chem.* **1987**, *91*, 6663.

(76) Bilewicz, R.; Majda, M. *J. Am. Chem. Soc.* **1991**, *113*, 5464.

(77) Chidsey, C. E. D. *Science* **1991**, *251*, 919.

(78) Becka, A. M.; Miller, C. J. *J. Phys. Chem.* **1992**, *96*, 2657.

(79) Finklea, H. O.; Hanshew, D. D. *J. Am. Chem. Soc.* **1992**, *114*, 3173.

(80) Dermody, D. L.; Crooks, R. M.; Kim, T. submitted for publication in *J. Am. Chem. Soc.*

(81) Menon, V. P.; Martin, C. R. *Anal. Chem.* **1995**, *67*, 1920.

(82) Poirier, G. E.; Tarlov, M. J.; Rushmeier, H. E. *Langmuir* **1994**, *10*, 3383.

(83) Li, J.; Liang, K.; Camillone, N.; Leung, T.; Scoles, G. *J. Chem. Phys.* **1995**, *102*, 5012-5028.

(84) McCarley, R. L.; Dunaway, D. J.; Willicut, R.J. *Langmuir* **1993**, *9*, 2775.

(85) Groat, K. A.; Creager, S. E. *Langmuir* **1993**, *9*, 3668.

Table 1. FTIR-ERS peak assignments of DA-COOH, MUA, DA-OH, MUD, and DA-CH_3 before and after exposure to UV light.

	ν_s (CH_2)/(fwhm), cm^{-1}	ν_a (CH_2)/(fwhm), cm^{-1}	ν (C=O)/(fwhm), cm^{-1}
Figure 1 - DA-COOH			
before UV	2856 / (18)	2930 / (32)	1719 / (26)
after UV	2856 / (20)	2926 / (29)	1719 / (58)
Figure 2 - MUA			
before UV	2856 / (21)	2926 / (29)	1719 / (19)
after UV	2856 / (20)	2926 / (27)	1719 / (20)
Figure 3 - DA-OH			
before UV	2856 / (18)	2927 / (32)	a
after UV	2858 / (18)	2928 / (34)	a
Figure 4 - MUD			
before UV	2854 / (17)	2924 / (30)	a
after UV	2856 / (23)	2922 / (28)	a
Figure 5 - DA-CH_3			
before UV	2857 / (15)	2927 / (27)	a
after UV	2856 / (15)	2926 / (35)	a
EC -32	2856 / (18)	2927 / (35)	a

a. Values not determined.

Table 1/Kim et al.

Figure Captions

Figure 1. FTIR-ERS spectra of a $HS(CH_2)_{10}C{\equiv}CC{\equiv}C(CH_2)_{10}COOH$ SAM-modified Au surface before (DA-COOH) and after (PDA-COOH) UV-light-induced polymerization.

Figure 2. FTIR-ERS spectra of a $HS(CH_2)_{10}COOH$ (MUA) SAM-modified Au surface before and after UV irradiation.

Figure 3. FTIR-ERS spectra of $HS(CH_2)_{10}C{\equiv}CC{\equiv}C(CH_2)_{10}CH_2OH$ SAM-modified Au surface before (DA-OH) and after (PDA-OH) UV-light-induced polymerization.

Figure 4. FTIR-ERS spectra of $HS(CH_2)_{10}CH_2OH$ (MUD) SAM-modified Au surface before and after UV irradiation.

Figure 5. FTIR-ERS spectra of $HS(CH_2)_{10}C{\equiv}CC{\equiv}C(CH_2)_{10}CH_3$ SAM-modified Au surface before ($DA-CH_3$) and after ($PDA-CH_3$) UV-light-induced polymerization. The bottom spectrum (EC-32) is that of a $PDA-CH_3$ SAM after 32 cyclic voltammetric scans between -0.5 and -1.4 V (vs. Ag/AgCl (3 M NaCl)) at 50 mV/s in an electrolyte consisting of a 1:1 mixture of 1.0 M aqueous KOH and ethanol.

Figure 6. SERS spectra for SAMs of (a) DA-COOH, (b) DA-OH, and (c) $DA-CH_3$ on roughened Au surfaces after 10 min irradiation with UV light.

Figure 7. (Top) Transmission UV-vis spectra of partially and fully polymerized, acid-terminated DA SAMs confined to semi-transparent Au thin films. UV-vis spectra are shown for UV illumination times of 3, 5, 7, and 13 min. (Bottom) Absorbance (at λ_{max}) normalized to the absorbance measured for a fully polymerized film vs. irradiation time for the acid-terminated DA SAM. The data points represented by large boxes correspond to the spectra shown at the top of the figure and the small boxes correspond to spectra (not shown) obtained at intermediate times.

Figure 8. (Top) Transmission UV-visible spectra of partially and fully polymerized, hydroxyl-terminated DA SAMs confined to semi-transparent Au thin films. UV-vis spectra are shown for UV illumination times of 2, 5, 7, and 10 min. (Bottom) Absorbance (at λ_{max}) normalized to the absorbance measured for a fully polymerized film vs. irradiation time for the hydroxyl-terminated DA SAM. The data points represented by large boxes correspond to the spectra shown at the top of the figure and the small boxes correspond to spectra (not shown) obtained at intermediate times.

Figure 9. Double-layer capacitance measurements for hydroxyl- (top) and acid- (bottom) terminated diacetylenic SAMs. The dashed and solid lines refer to the SAMs before and after polymerization, respectively. Conditions: electrolyte solution, aqueous 0.1 M KCl; scan rate = 100 mV/s; active electrode area 0.70 cm^2.

Figure 10. Cyclic voltammograms corresponding to $Ru(NH_3)_6^{3+}$ permeability through hydroxyl- (top) and acid- (bottom) terminated diacetylenic SAMs. The dashed and solid lines refer to the SAMs before and after polymerization, respectively. Conditions: electrolyte solution, aqueous 0.1 M KCl plus 5 mM $Ru(NH_3)_6Cl_3$; scan rate = 50 mV/s; active electrode area 0.70 cm^2.

Figure 11. FTIR-ERS spectra for HDT, DA-COOH, and PDA-COOH SAMs on Au electrodes after 0, 2, and 16 reductive desorption cyclic voltammetric scans. All electrodes were scanned between -0.5 and -1.4 V (vs. Ag/AgCl (3 M NaCl)) at 50 mV/s in an electrolyte consisting of a 1:1 mixture of 1.0 M aqueous KOH and ethanol.

Figure 12. Fractional change in $\nu_a(CH_2)$ peak intensity vs. the number of cyclic voltammetric scans for SAMs composed of HDT, DA-COOH, and PDA-COOH.

Figure 13. FTIR-ERS spectra for HDT, DA-COOH, and PDA-COOH SAMs on Au electrodes after exposure to flowing Ar at 200 °C for 0, 2, and 5 min.

Figure 14. FTIR-ERS spectra for HDT and PDA-COOH SAMs on Au surfaces after exposure to a solution consisting of a 1:1 mixture of ethanol and 1.0 M aqueous KOH at 100 °C for 0 and 2 min.

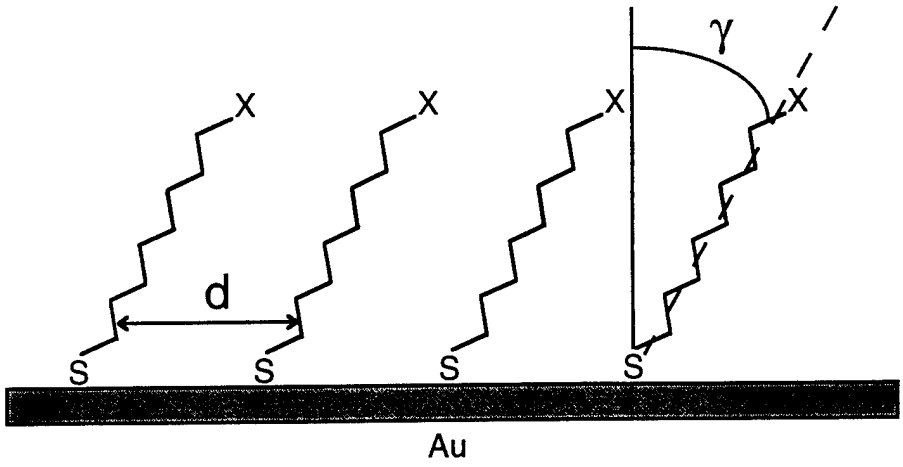

d	4.99 Å
γ	30 - 40°

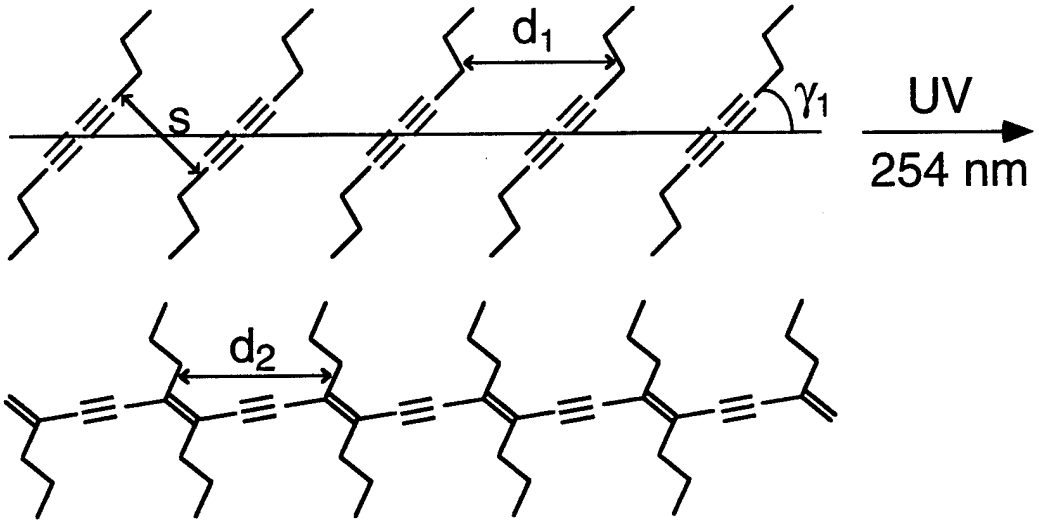

s	3.4 - 4.0 Å
d_1	4.7 - 5.2 Å
d_2	4.93 Å
γ_1	about 45° ,s = $d_1 \sin \gamma$

Scheme I/Kim et al.

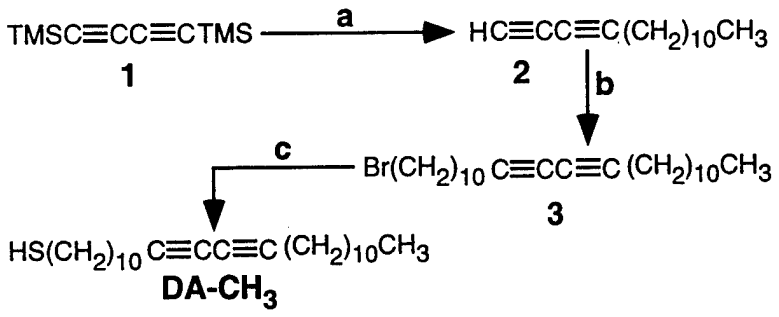

a. 1 equiv of 1.5 M MeLi/LiBr, THF, -78 °C; $Br(CH_2)_{10}CH_3$/HMPA:

b. 1 equiv of 1.6 M BuLi, THF, 0 °C; 5 equiv of $Br(CH_2)_{10}Br$/HMPA, rt:

c. 6 equiv of NaSH/EtOH, 50-55 °C, 4 h, sonication

Scheme II/Kim et al.

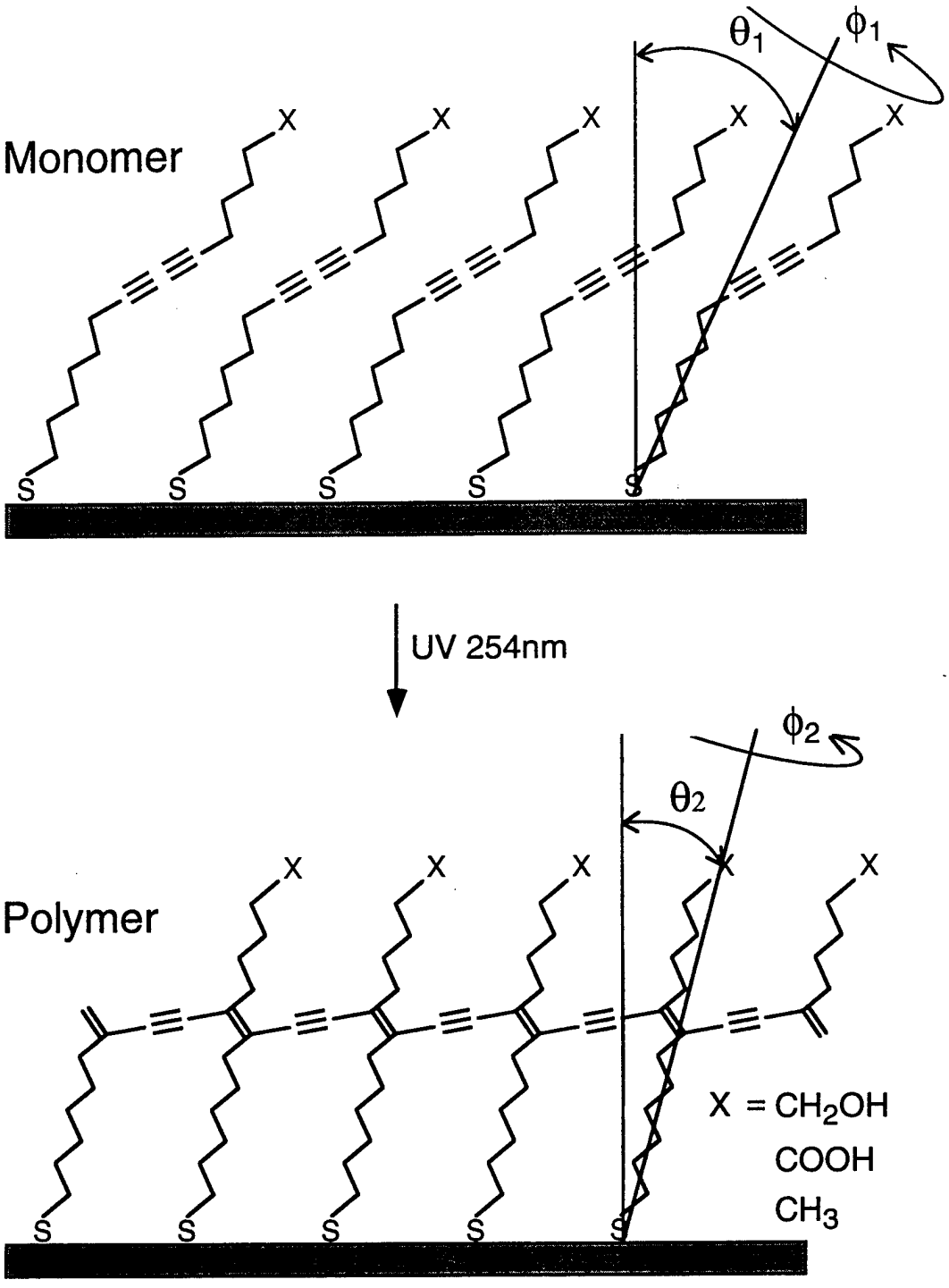

$\theta_2 < \theta_1$ - untilting

$\phi_2 < \phi_1$ - untwisting

Scheme III/Kim et al.

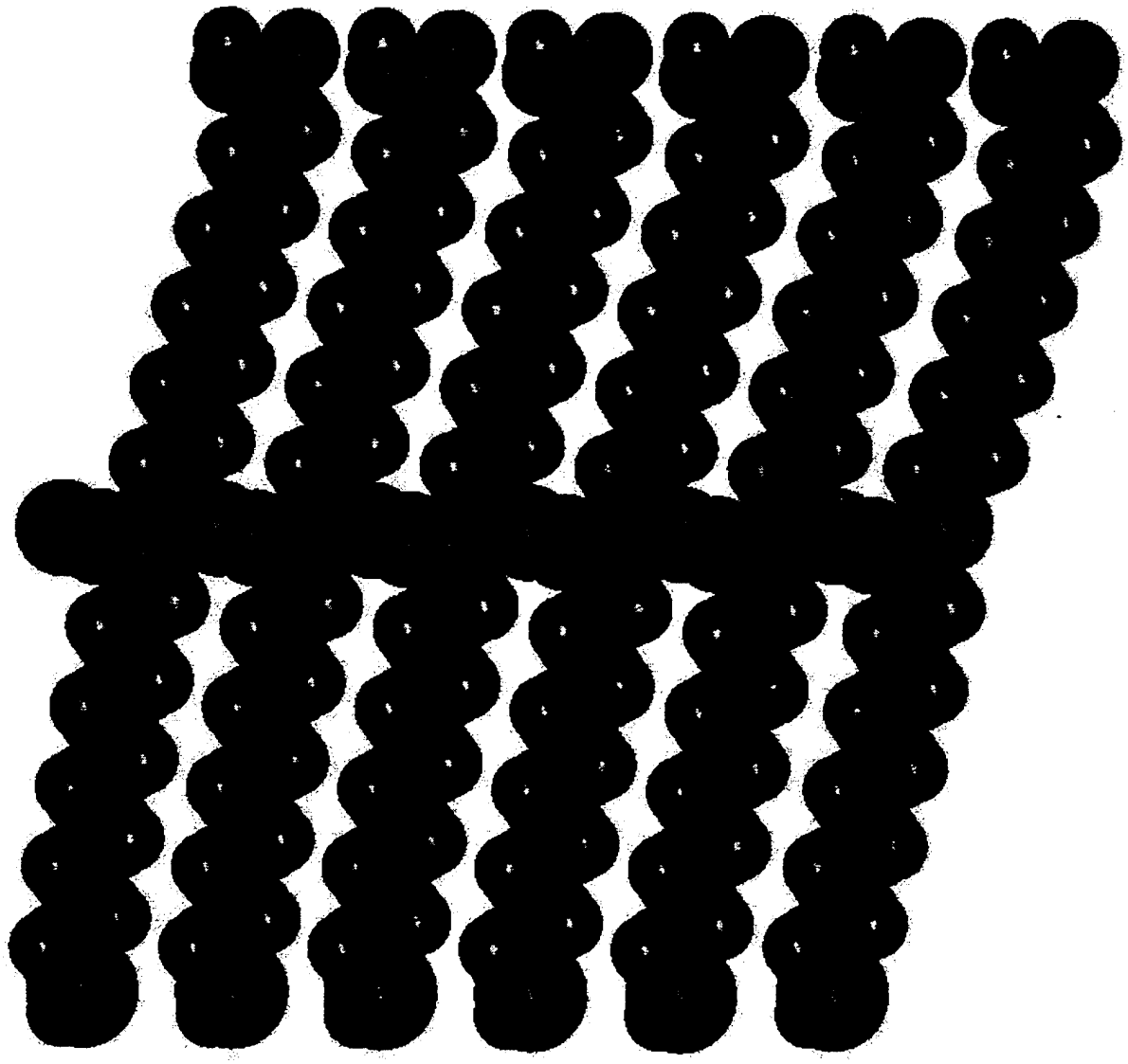

Scheme 4/Kim et al.

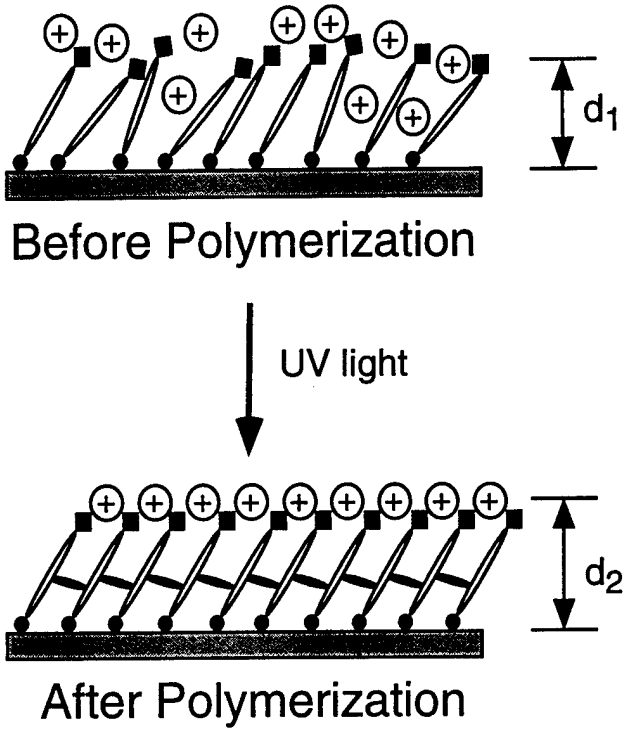

Scheme V/Kim et al.

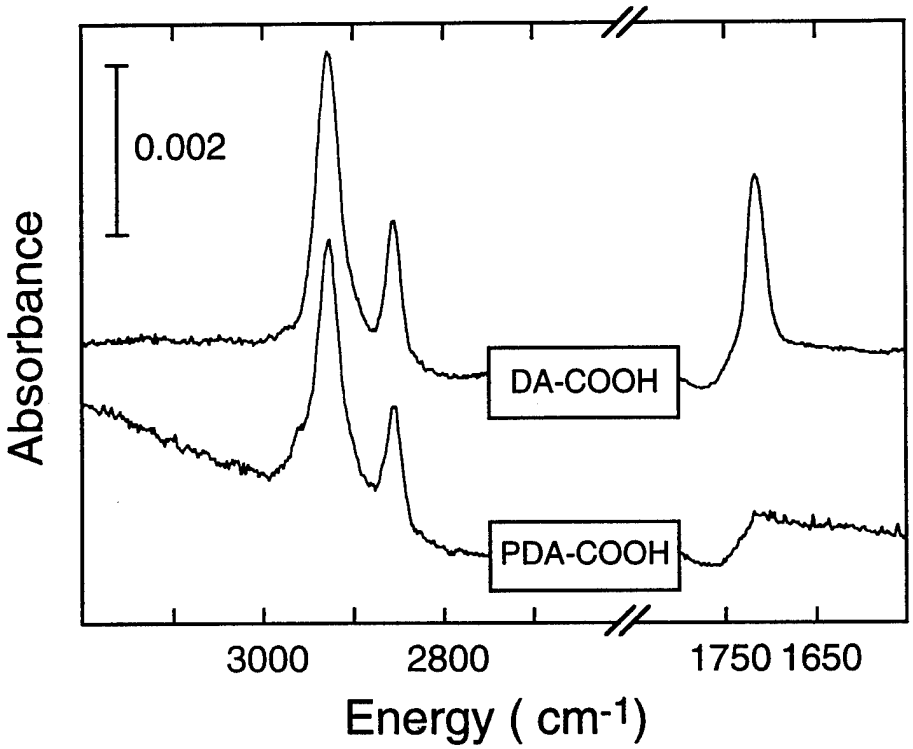

Fig 1/Kim et al.

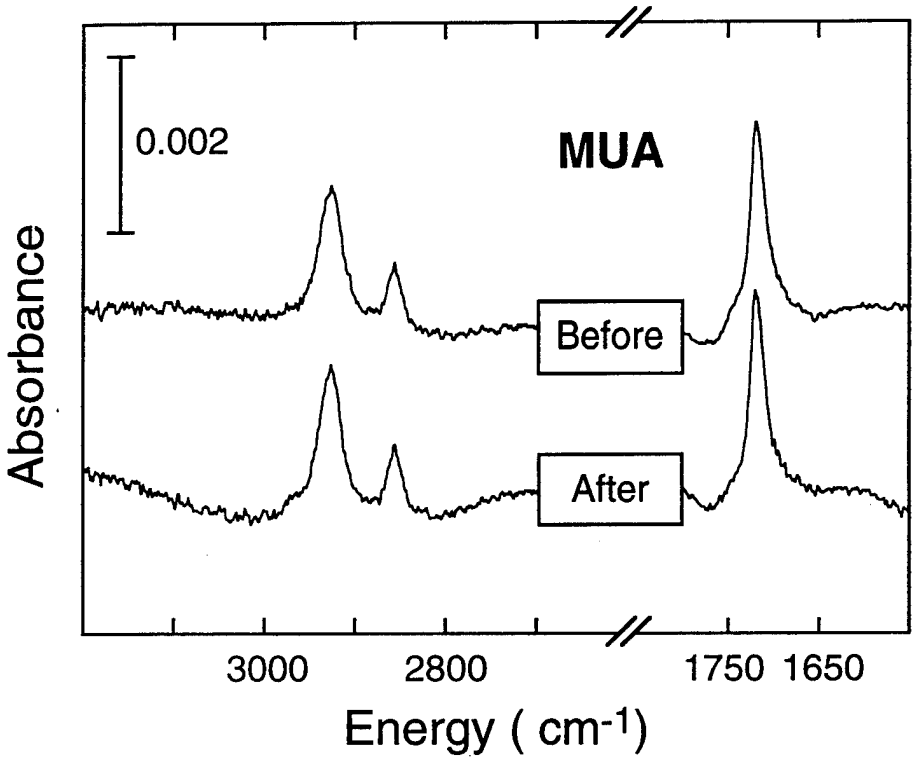

Fig 2/Kim et al.

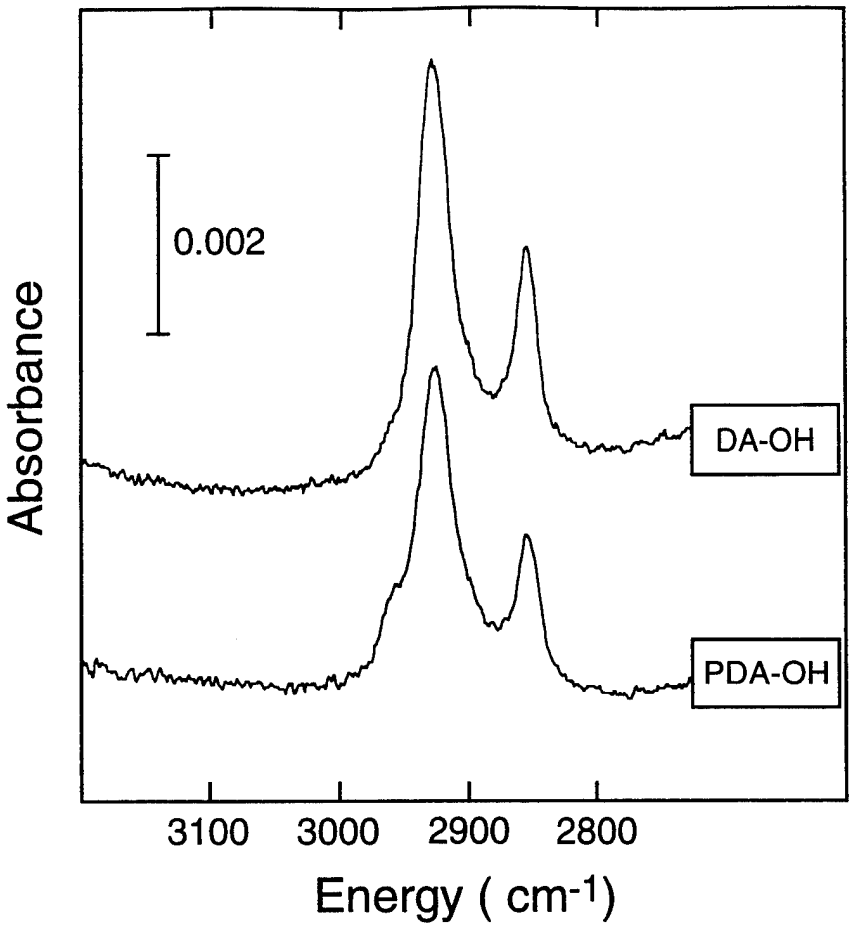

Fig 3/Kim et al.

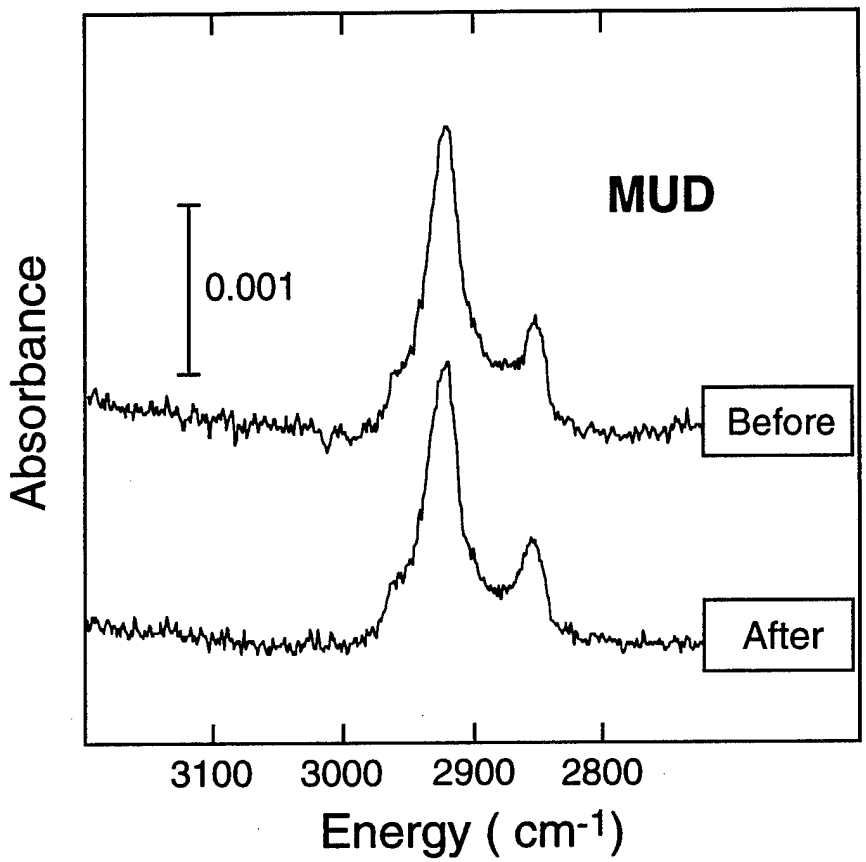

Fig 4/Kim et al.

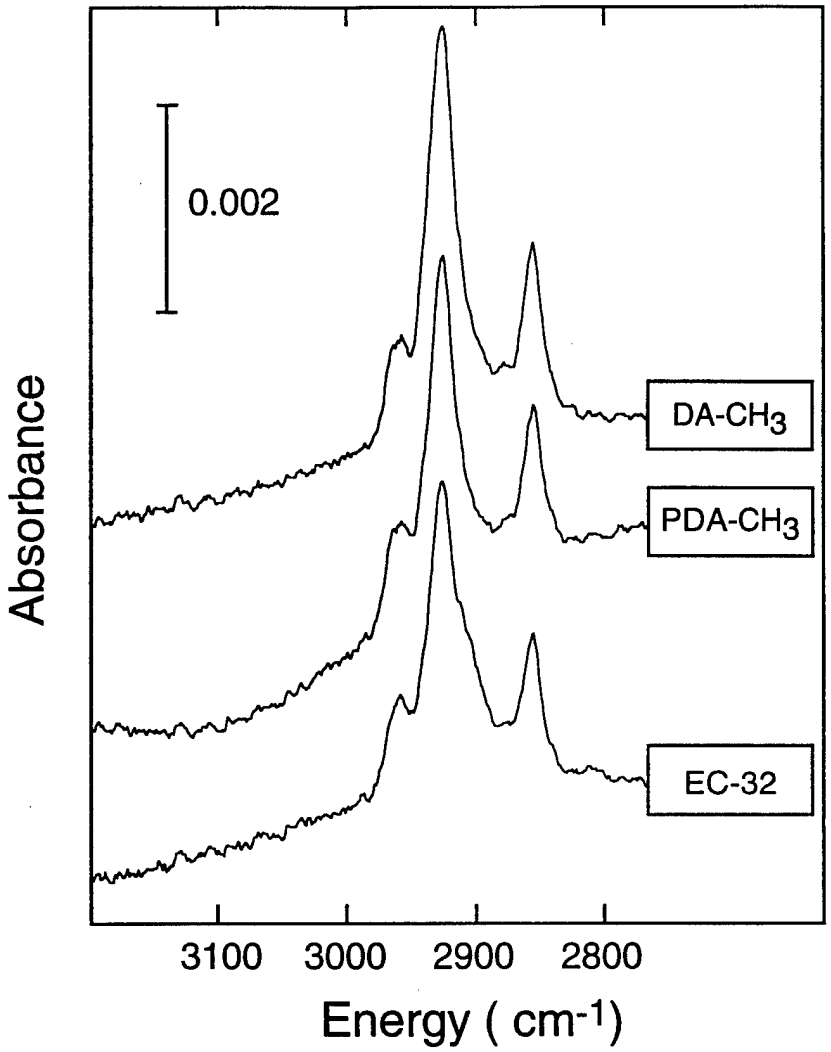

Fig 5/Kim et al.

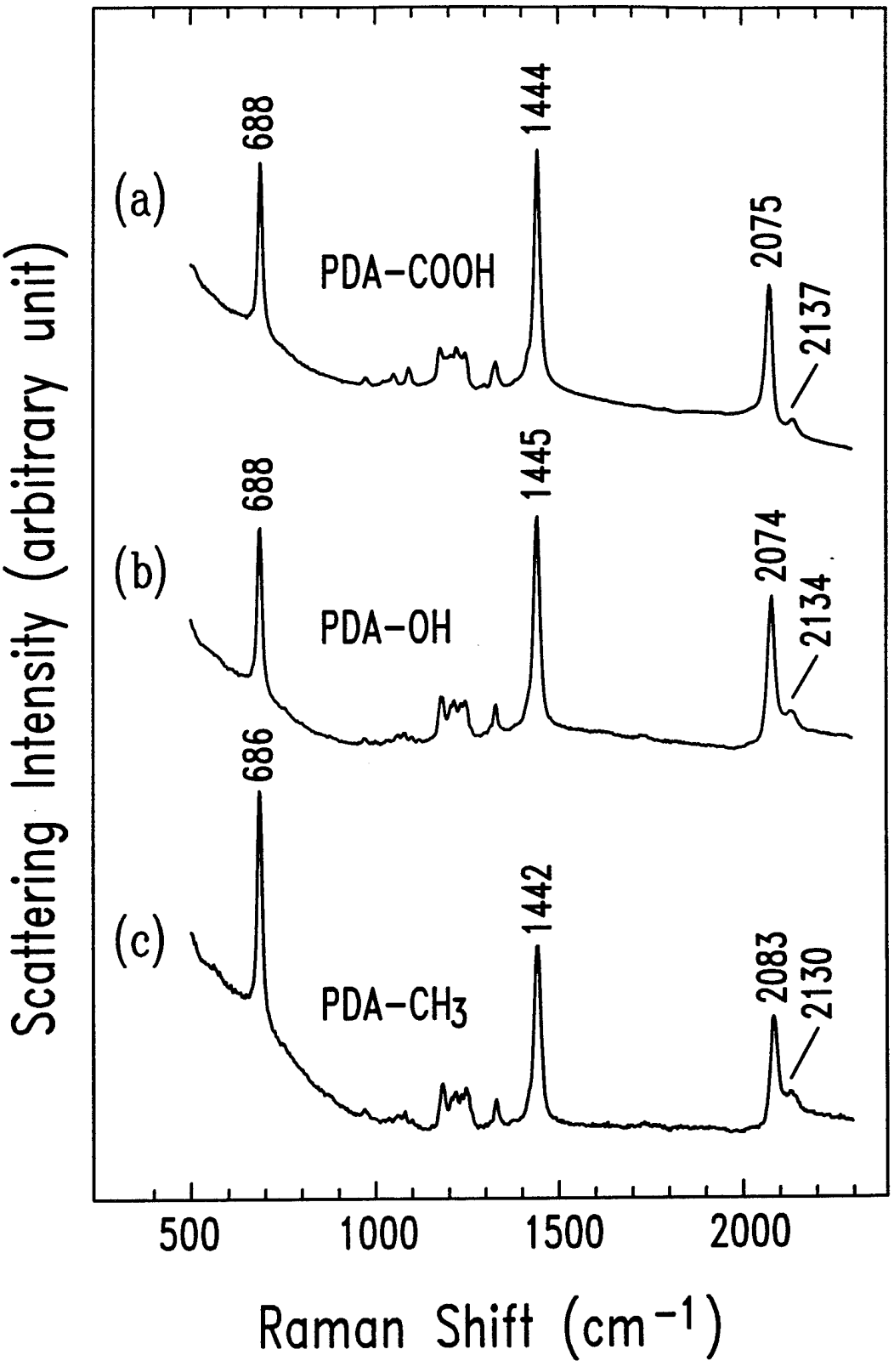

Fig 6 / Kim et al.

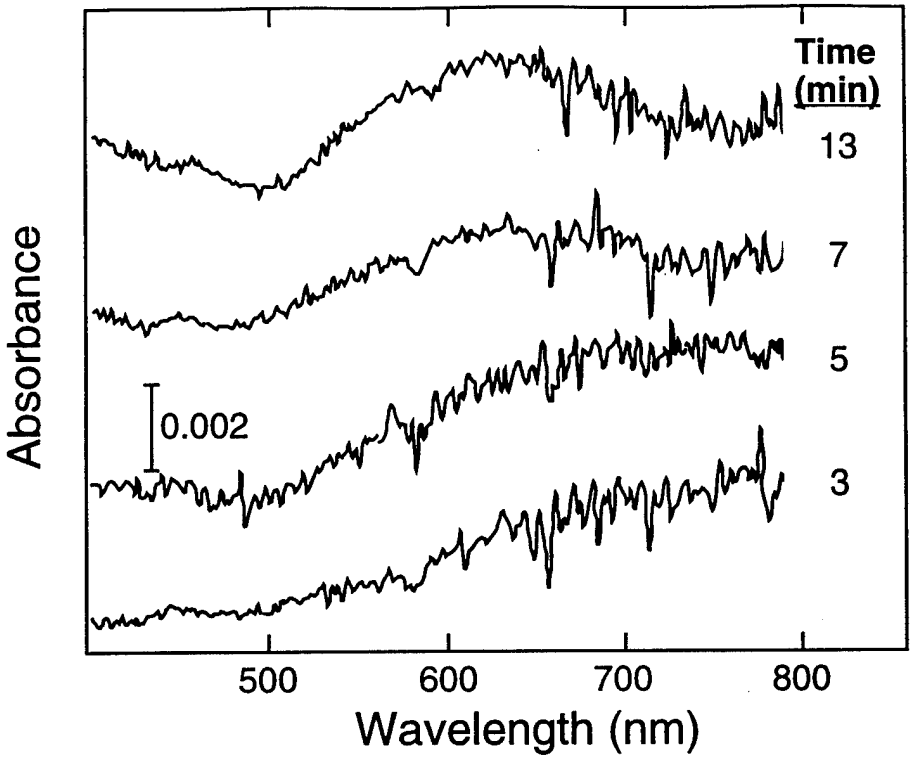

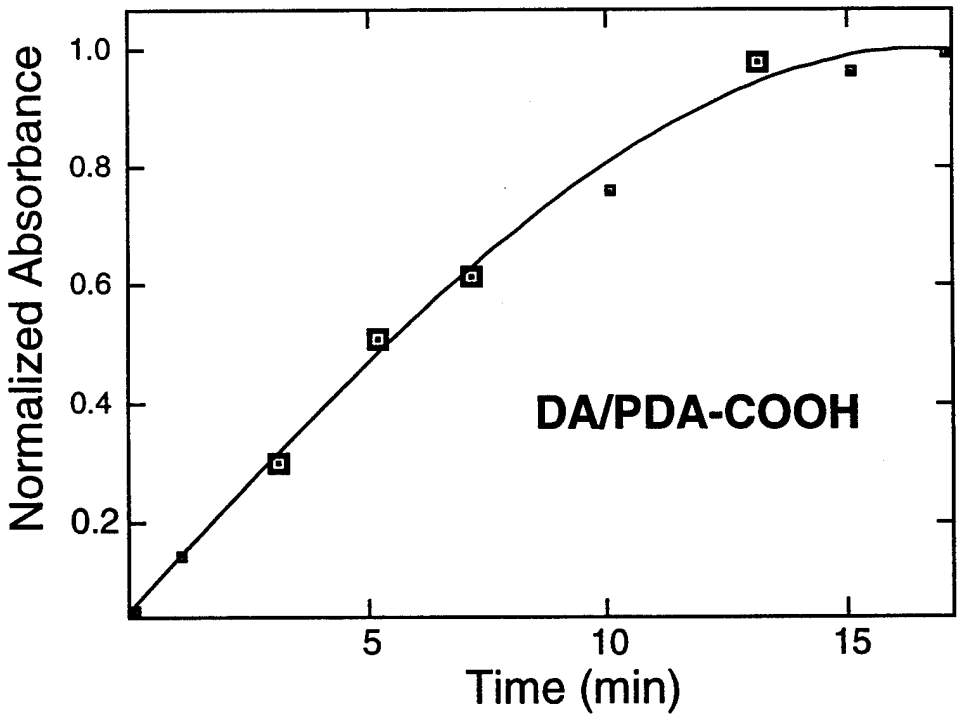

Fig 7/Kim et al.

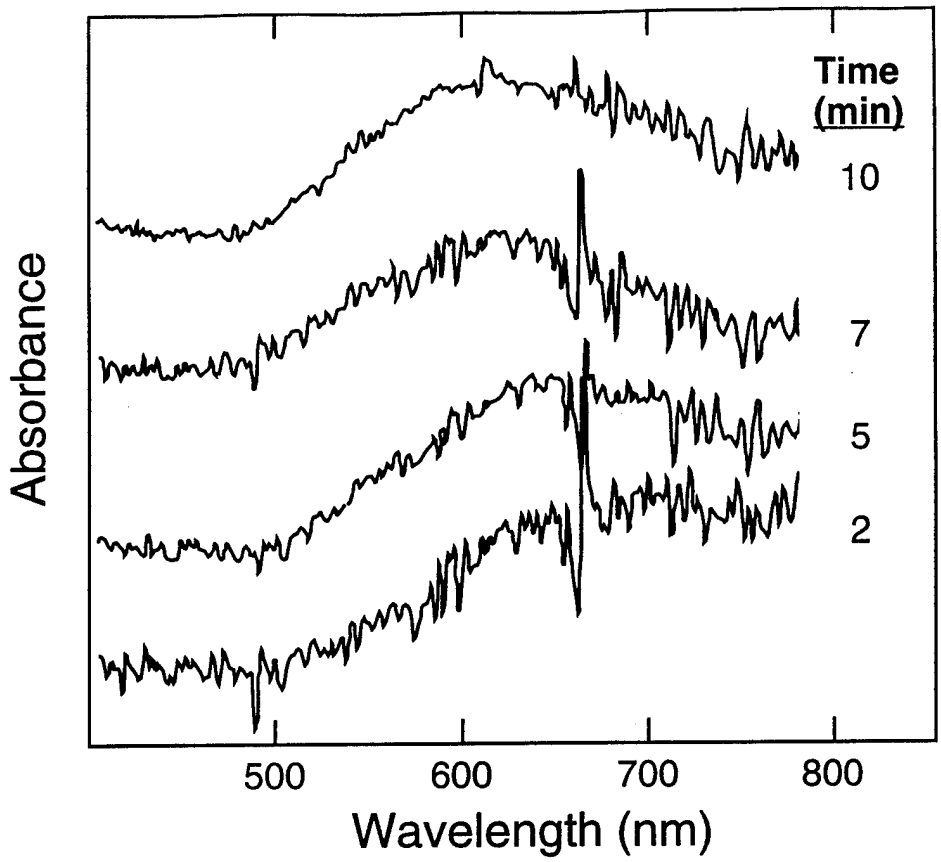

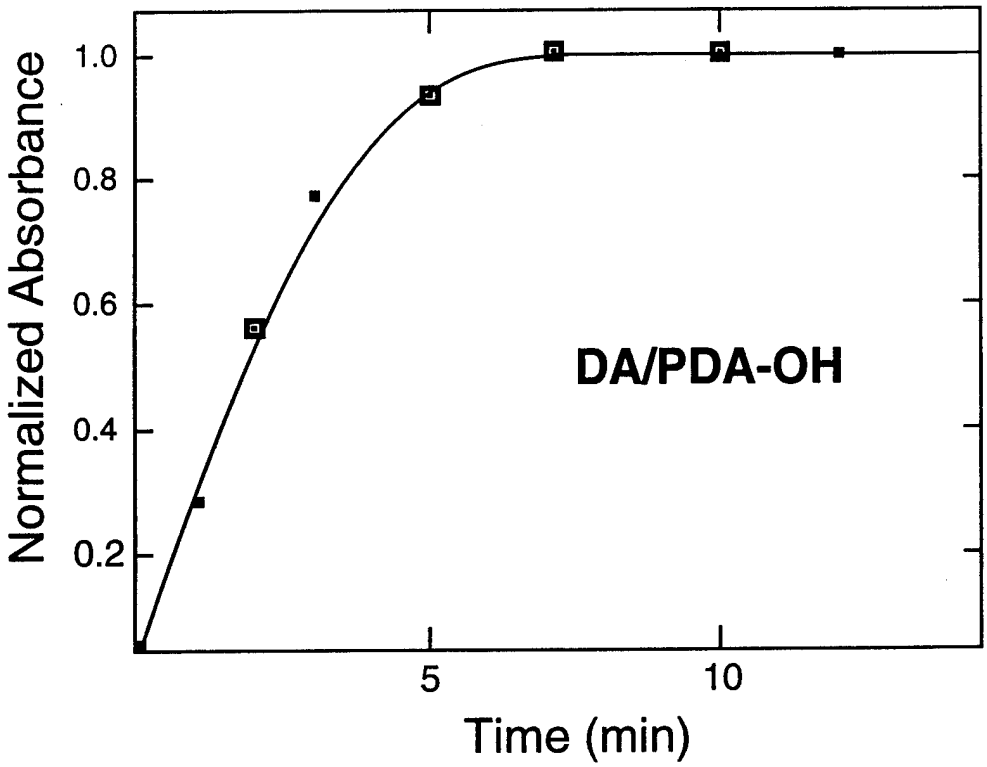

Fig 8/Kim et al.

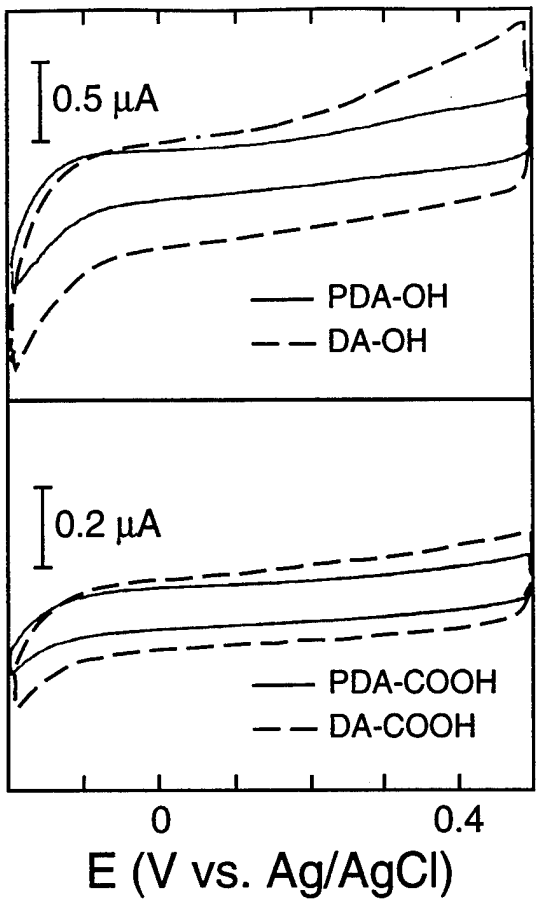

Figure 9/Kim et al.

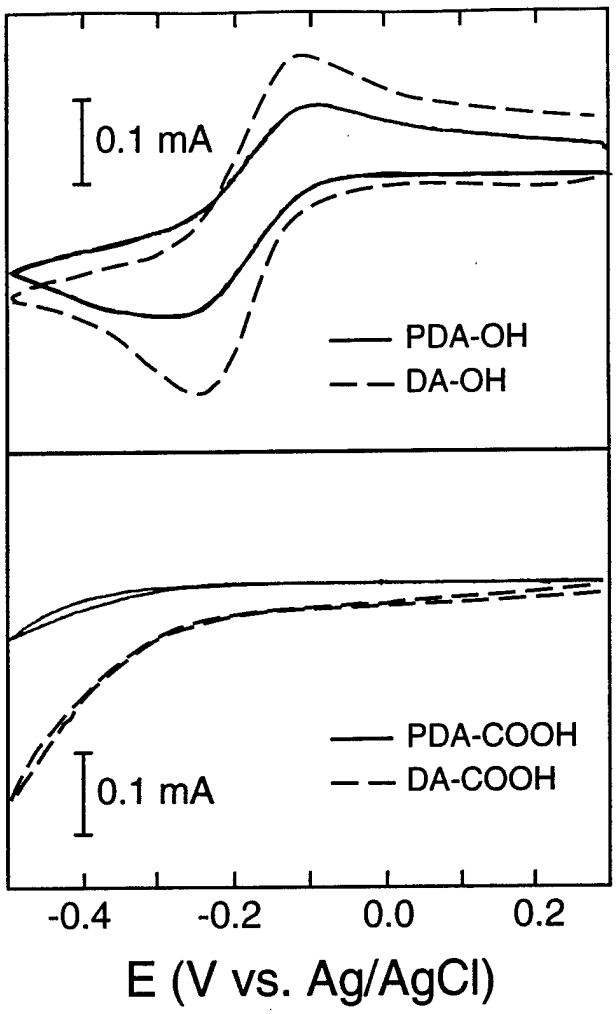

Fig 10/Kim et al.

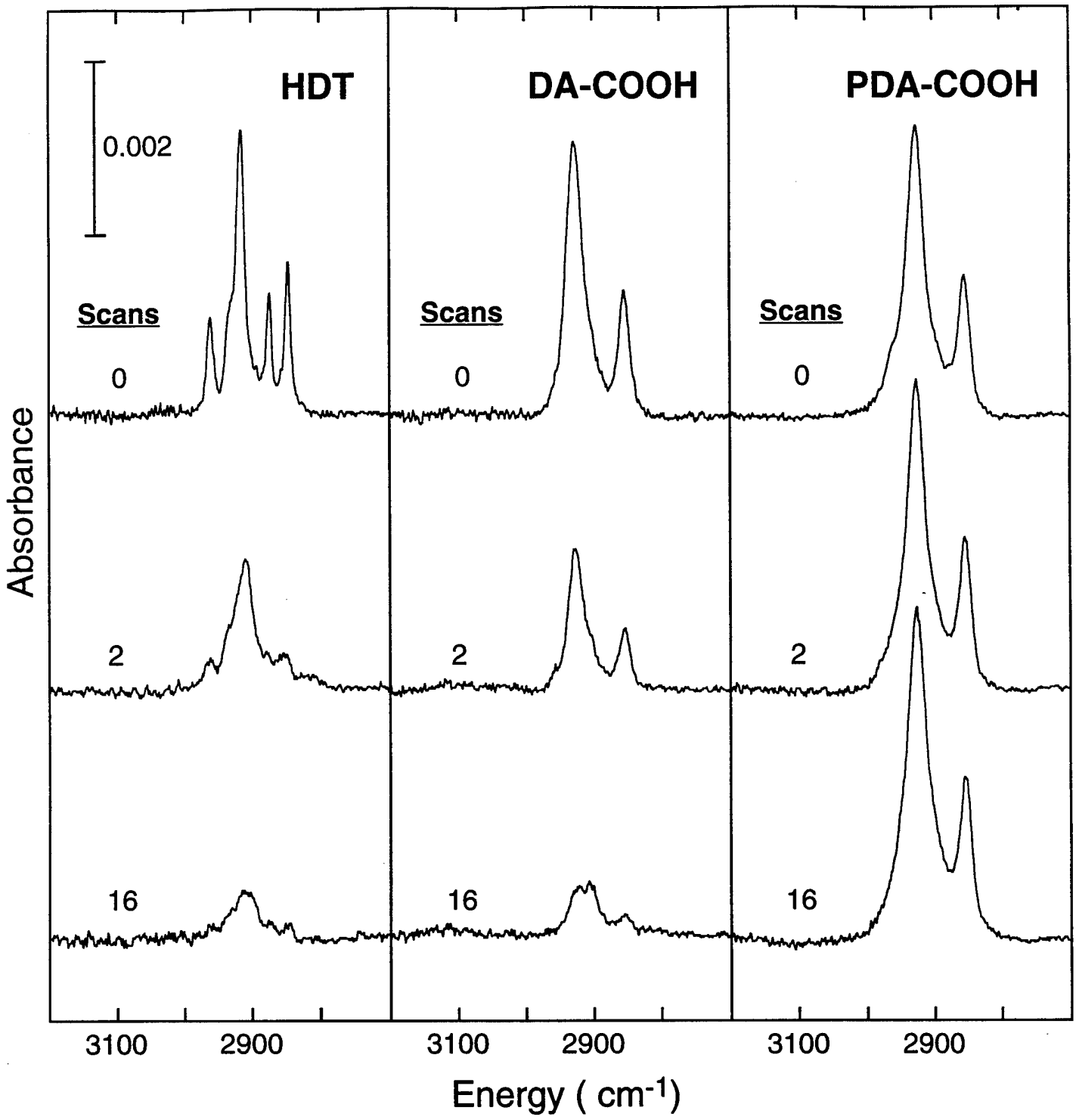

Fig 11/Kim et al.

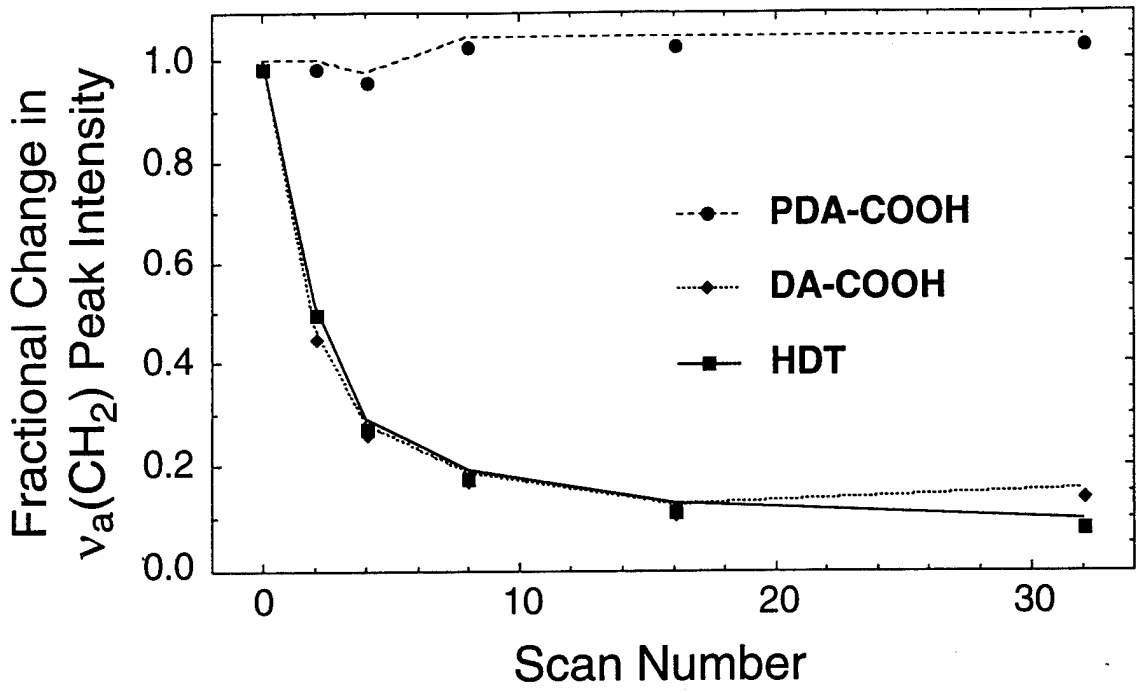

Fig 12/Kim et al.

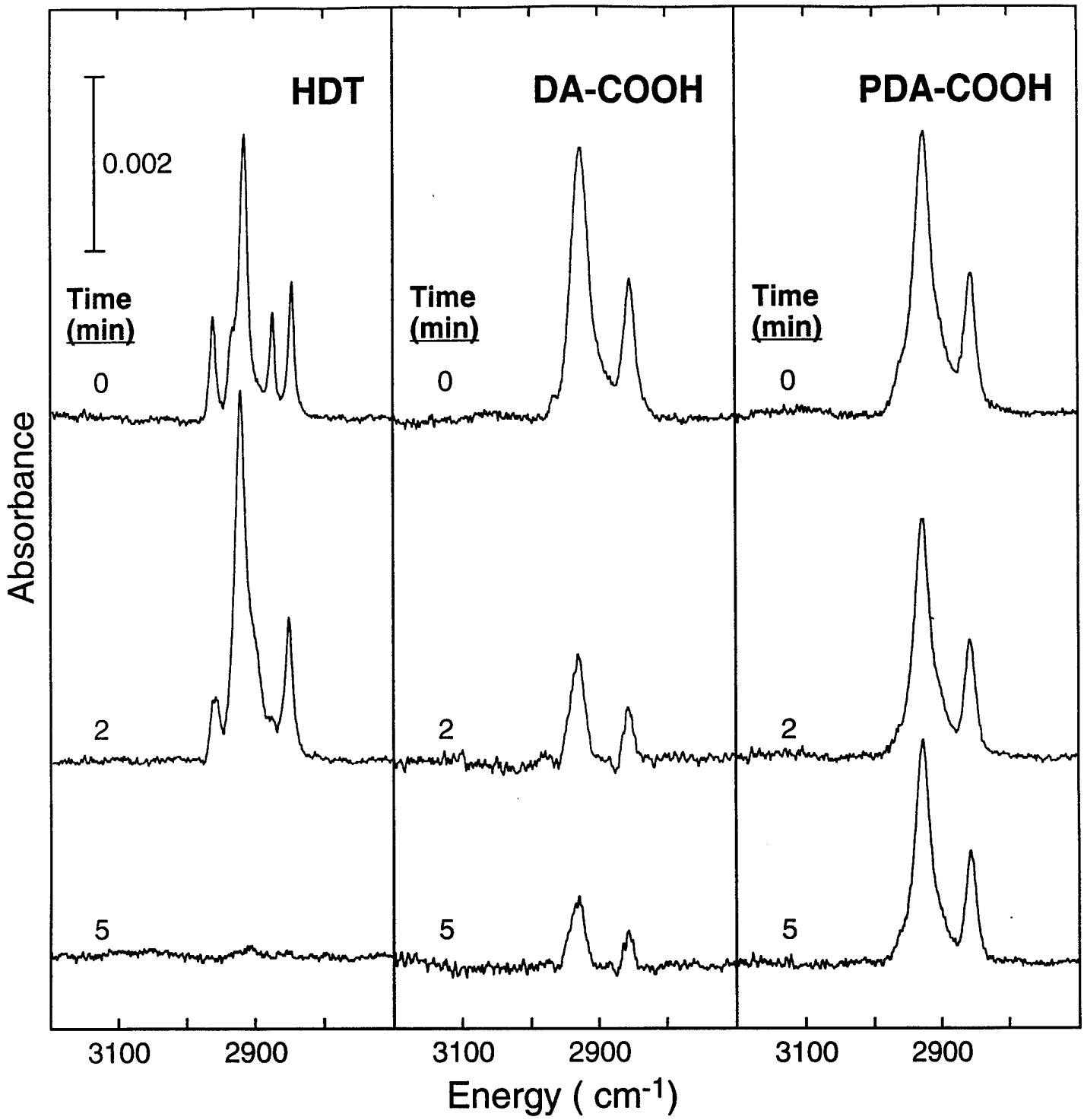

Fig 13/Kim et al.

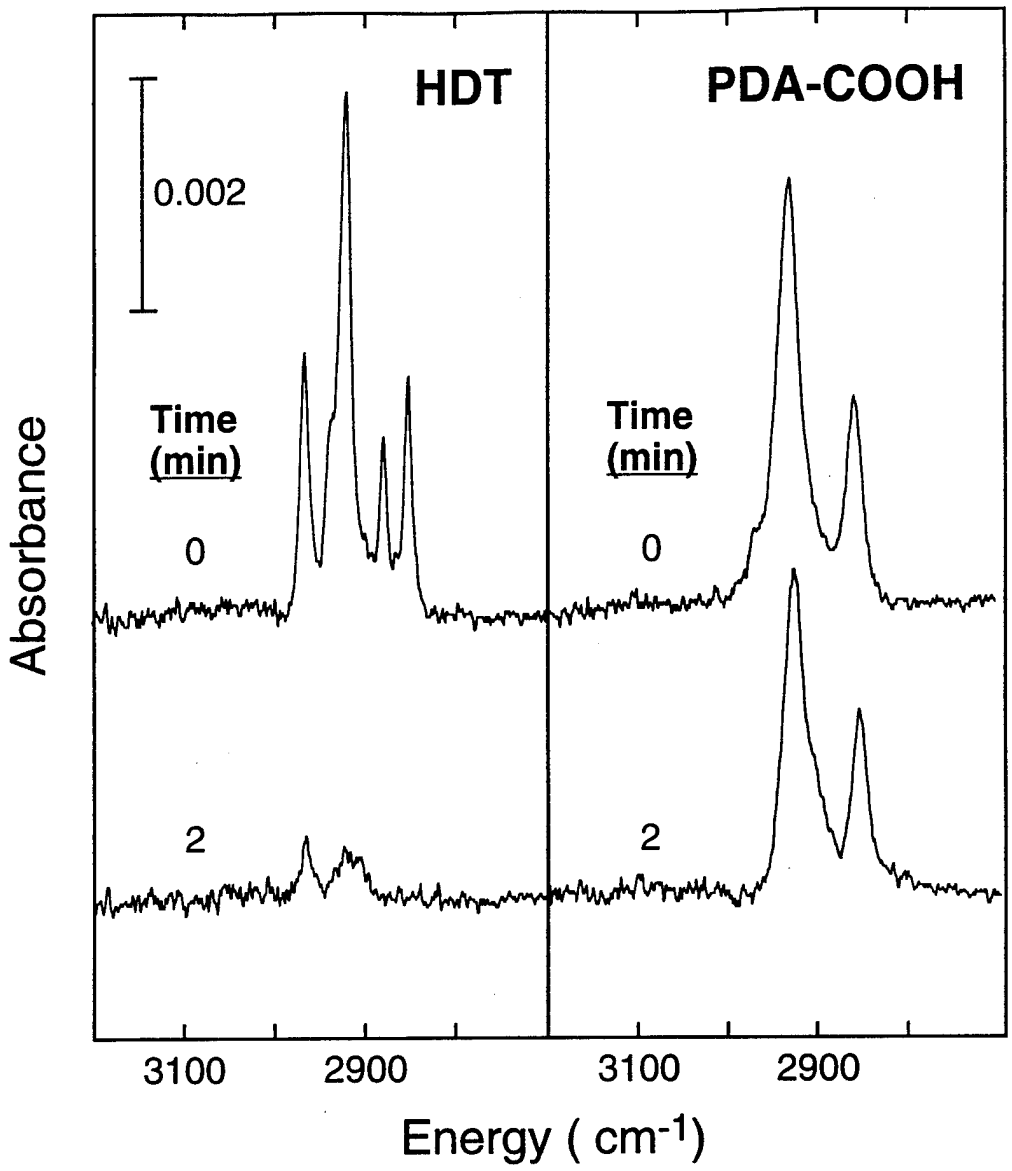

Fig 14/Kim et al.